Baseload electricity and hydrogen supply based on hybrid PV-wind power plants

Mahdi Fasihi[*], Christian Breyer

LUT University, Yliopistonkatu 34, 53850, Lappeenranta, Finland

ABSTRACT

The reliable supplies of electricity and hydrogen required for 100% renewable energy systems have been found to be achievable by utilisation of a mix of different resources and storage technologies. In this paper, more demanding parameter conditions than hitherto considered are used in measurement of the reliability of variable renewable energy resources. The defined conditions require that supply of baseload electricity (BLEL) and baseload hydrogen (BLH$_2$) occurs solely using cost-optimised configurations of variable photovoltaic solar power, onshore wind energy and balancing technologies. The global scenario modelling is based on hourly weather data in a $0.45° \times 0.45°$ spatial resolution. Simulations are conducted for *Onsite* and *Coastal Scenarios* from 2020 to 2050 in 10-year time-steps. The results show that for 7% weighted average cost of capital, *Onsite* BLEL can be generated at less than 119, 54, 41 and 33 €/MWh$_{el}$ in 2020, 2030, 2040 and 2050, respectively, across the best sites with a maximum 20,000 TWh annual cumulative generation potential. Up to 20,000 TWh$_{H2,HHV}$ *Onsite* BLH$_2$ can be produced at less than 66, 48, 40 and 35 €/MWh$_{H2,HHV}$, in 2020, 2030, 2040 and 2050, respectively. A partially flexible electricity demand at 8000 FLh, could significantly reduce the costs of electricity supply in the studied scenario. Along with battery storage, power-to-hydrogen-to-power is found to have a major role in supply of BLEL beyond 2030 as both a daily and seasonal balancing solution. Batteries are not expected to have a significant role in the provision of electricity to water electrolysers.

© 2019 The Authors. Published by Elsevier Ltd. This is an open access article under the CC BY license (http://creativecommons.org/licenses/by/4.0/).

1. Introduction

Access to reliable sources of electricity and hydrogen, as energy carriers or feedstock, is essential for sectors with low flexibility and in industries that favour baseload operation to boost production and profitability. This demand for electricity and hydrogen has thus far been met mainly by fossil and nuclear fuels, both of which have severe sustainability and economic limitations (Child et al., 2018). Furthermore, the use of fossil fuels increases global greenhouse gas emissions and their continued use is contrary to the provisions of the Paris Agreement (UNFCCC, 2015; IPCC, 2018).

Of the currently economically feasible renewable energy options, hydropower (IHA, 2019), geothermal (IRENA, 2017), concentrated solar thermal power (Pitz-Paal, 2017) and bioenergy (IEA Bioenergy, 2017) have the potential to provide reliable electricity seasonally or throughout the year; however, their capacities are relatively limited and are location-dependent. On the other hand,

solar and wind energy are abundant resources but lack reliability due to their variable nature (IPCC, 2012).

Baseload generation is considered the backbone of the electricity grid by some scientists. In this view, the uninterrupted capacity of baseload electricity helps provide grid stability and reliability in an electricity system with a high share of variable renewable energy (Squalli, 2017) as strengthening the reliability and security of the grid by electricity storage is considered an expensive option (Dunn et al., 2011). On the other hand, coupling the system with conventional dispatchable resources would limit possible emission cuts (Reichenberg et al., 2018). In recent years, however, the drop in the cost of variable renewable energy and storage options, as well as resource integration, are calling into question the need for significant volumes of baseload generation. Studies show that grid demand could be supplied by a mix of different renewable resources and storage options (Brown et al., 2018; Hansen et al., 2019), even if bioenergy is avoided (Jacobson et al., 2018), making a 100% renewable power sector technically feasible and economically viable globally (Bogdanov et al., 2019).

Nevertheless, baseload electricity (BLEL) supply can be

Nomenclature

BLEL	Baseload Electricity
BLH_2	Baseload Hydrogen
capex	Capital Expenditures
FLh	Full Load hours
GT	Gas Turbine
HVAC	High-Voltage Alternating Current
HVDC	High-Voltage Direct Current
LCOBLEL	Levelised Cost of Baseload Electricity
$LCOBLH_2$	Levelised Cost of Baseload Hydrogen
LCOE	Levelised Cost of Electricity
opex	Operating Expenditures

PV	Photovoltaic
RE	Renewable Energy
SMR	Steam Methane Reforming
SNG	Synthetic Natural Gas
WACC	Weighted Average Cost of Capital

Subscripts

el	electricity
fix	fixed
rp	rated power
th	thermal
var	variable

---

considered as a benchmark for reliability assessment of power supply from different mixes of resources and technologies in different climates, as well as a reference for potential BLEL demand. Mason and Archer (2012) investigated the possibility of baseload electricity from wind via compressed air energy storage in the USA. Shokrzadeh et al. (2015) estimated the energy storage capacity for baseload wind power generation from an energy efficiency perspective. Pfenninger and Keirstead (2015) compared concentrating solar power and nuclear power as baseload electricity providers for South Africa.

The above-mentioned studies differ in the technologies applied or are limited to specific geographical regions, and the concept of baseload electricity from variable renewables (mainly solar and wind) on a global scale and in high spatial resolution has not been comprehensively researched and discussed in scientific literature. Thus, this study examines the global feasibility of BLEL by cost-optimised large-scale islandic hybrid PV-wind systems as the sole source of electricity coupled with battery and power-to-hydrogen-to-power systems as globally accessible balancing options. Since the study aims at a global evaluation of solar and wind reliability, the system excludes regionally available resources or storage options.

New power demand is arising with the expansion of RE beyond the power sector. Such demand could be centred on specific regions without a grid connection, due to additional load or long distances, for example, water desalination units in coastal areas (Caldera et al., 2016), or CO_2 Direct Air Capture units in the desert (Breyer et al., 2019a). Although these systems are capable of flexible operation, studies have shown that for economic reasons such capital expenditure (capex) intensive plants favour high full load hours (FLh) even at high electricity prices (Caldera and Breyer, 2018; Fasihi et al., 2019). Thus, we also study the costs of close-to-baseload (8000 full load hours) off-grid power systems.

Apart from the power sector, a transition to a 100% renewable energy system (Hansen et al., 2019) will require defossilisation of energetic and non-energetic use of hydrocarbons, for which a sustainable and reliable hydrogen supply will be required (Teske, 2019; Ram et al., 2019). Such hydrogen demand includes hydrogen used as feedstock in the chemical industry (DECHEMA, 2017), hydrogen needed in future steel industry (Otto et al., 2017) and in the production of synthetic fuels and bulk chemicals, such as synthetic methanol (Anicic et al., 2014), ammonia (Valera-Medina et al., 2018), methane, naphtha, diesel and kerosene (Fasihi et al., 2017). Flexible water electrolysers (Millet and Grigoriev, 2013) can generate hydrogen whenever renewable electricity is available, however, the chemical industry and most of the synthetic fuel production plants are designed to work on baseload. Thus, access to baseload hydrogen (BLH_2) is crucial. In this regard, we also investigate the overall costs of RE-BLH_2 via cost-optimised hybrid PV-wind-battery systems, with hydrogen storage in well-known salt caverns (Ozarslan, 2012).

In the case of land limits or high costs of local supply, electricity generated in remote areas can be transmitted to demand sites for direct consumption or for hydrogen generation. Coastal areas could be major importers as they tend to have high population density (Gao, 2019) and, consequently, a higher energy demand. In addition, some industrial processes such as seawater desalination plants, inherently, need to be located at the coast regardless of the demand location. Moreover, for intercontinental export of energy from the best solar and wind sites in the world, one option is to transmit the electricity to the coast and then convert it to fuels or bulk chemicals suitable for shipping via Power-to-X facilities located at the coast, as studied for the case of Australia (Gulagi et al., 2017), the Maghreb region (Fasihi et al., 2017), the Americas (Aghahosseini et al., 2019), and the Pacific Rim (Heuser et al., 2019). As mentioned earlier, such processes are typically designed to run on a baseload and thus need access to baseload hydrogen (Fischer-Tropsch process, methanol synthesis, ammonia synthesis) or partly baseload electricity (ammonia synthesis). Consequently, the costs of delivering BLEL and BLH_2 to the nearest coast have been investigated in this study as well. In addition, the cost difference of *Onsite* and *Coastal Scenarios* could be used as a measure for delivery costs of final products to other on-land destinations that are at the same distance.

Hydrogen pipelines could be another option for energy transportation to the coast (IEA, 2019). However, different terrain conditions around the globe have a big impact on the possibility and cost of hydrogen pipelines. Due to lack of access to proper geological data on a global scale we could not reflect such impacts in the results and thus this option has been excluded from this study.

In a fossil-based energy system, hydrogen is mainly derived from natural gas (NG) through steam methane reforming, which results in higher costs of H_2 in comparison to NG (Chisalita and Cormos, 2019), which makes NG-fuelled gas turbines (NG-GTs) more favourable. However, this trend is reversed in a RE-based system, as hydrogen generation by water electrolysis is cheaper than the production of synthetic natural gas (SNG) (Fasihi et al., 2017). This reversed trend has provided an incentive for development of hydrogen-fuelled gas turbines (H_2-GTs), which would also fully eliminate CO_2 from the cycle, resulting in a cleaner and simpler Power-to-X-to-Power chain. The concept of H_2-GTs has been proven and companies are working on commercialisation (Kawasaki, 2015; MHPS, 2018). Leading gas turbine technology providers have committed to meet customer demand for gas turbines operating with 100% hydrogen by 2030 (EUTurbines, 2019).

Furthermore, Siemens, with some turbines already capable of running on 100% hydrogen, has set a target of making all its turbines compatible with 100% hydrogen by 2030 (Siemens, 2019). Hydrogen fuel cells, as the other seasonal balancing solution, have a comparable efficiency to gas turbines, but their lifetime is expected to be shorter and their capex is significantly higher than that of gas turbines, which leads to higher levelised cost of electricity (LCOE) of fuel cells, compared to gas turbines (EC, 2014). Thus, hydrogen fuel cells have not been considered in this study.

The core focus of this paper is the analysis of BLEL and BLH$_2$ on a global-local scale based on variable solar PV and wind electricity supply. The applied methods and data are comprehensively explained in Section 2. Results are presented in Section 3 and are further discussed in Section 4. Conclusions are drawn in Section 5.

2. Methods and data

2.1. Methods

Two scenarios (*Onsite* and *Coastal*) are modelled to represent the local consumption and export cases.

In the *Onsite Scenario*, the final BLEL or BLH$_2$ demand is considered to be at the electricity generation site. Thus, all conversion and storage technologies are located at the same location. The schematics of the *Onsite* models are illustrated in Fig. 1.

Electricity is generated by the cost-optimised configuration of fixed tilted PV, single-axis tracking PV and wind turbines. The battery system consists of an independently scalable battery interface and battery storage to address both electrical power and energy storage in a cost-effective way. Along with batteries, a power-to-hydrogen-to-power (PtH$_2$tP) system is included in the BLEL model from 2030 onwards to balance the electricity generation. In this case, electricity is used for hydrogen generation via high pressure alkaline water electrolysers at 40 bar and is then stored in onsite man-made hydrogen caverns at an operating pressure of 60−200 bar via hydrogen compressors (Michalski et al., 2017). A fixed average electricity demand of 0.02 kWh/kWh$_{H2,HHV}$ is considered for isothermal compression of hydrogen in the range of

40−200 bar, according to Makridis (2016). Considering the relatively high pressure of the cavern, even at its minimum state of charge, no auxiliary compressor is included for hydrogen discharge from the cavern to H$_2$-GTs or to supply BLH$_2$ demand. Both open cycle and combined cycle gas turbines are included in the model for their relatively lower capital cost and higher conversion efficiency, respectively. As discussed in the introduction, H$_2$-GTs are expected to be commercially available by 2030. Thus, H$_2$-GTs are included in the model from 2030 onwards.

In the *Coastal Scenario*, illustrated in Fig. 2, electricity can be optionally balanced before reaching the transmission lines via battery or PtH$_2$tP technologies, if helpful for lowering the total system costs, and is then transmitted to the nearest coast. Another set of electricity and hydrogen balancing technologies are available after the transmission lines to provide baseload electricity or hydrogen at the coast. As in the *Onsite Scenario*, H$_2$-GTs have been excluded from the models in 2020. To roughly factor in natural barriers, the length of the transmission line is set at 110% of the direct distance to the nearest coast. Actual political and natural barriers, such as country borders, lakes and mountains, are not taken into account. Both high-voltage alternating current (HVAC) and high-voltage direct current (HVDC) options are included in the model. HVDC is more capex intensive but has lower losses, which makes it a potentially better option for long-distance electricity transmission at high full load hours (FLh).

In regions with water scarcity, the required water for electrolysers needs to be supplied from other regions or sources. According to Caldera et al. (2016), hybrid PV-wind systems could be used to power seawater desalination plants and water pumped to most areas with water scarcity at costs below 2 €/m^3 in 2030. This water cost would add less than 0.5 €/MWh$_{th}$ to the hydrogen generation cost in 2030. Lower costs could be expected for the years beyond, as the costs of RE are expected to decline as well as the capex of desalination plants (Caldera and Breyer, 2017). For the *Coastal Scenario*, desalinated water costs would be even lower, as the water pumping step would be eliminated. Thus, the cost of water has a negligible impact on the final cost of hydrogen generation. Therefore, for the sake of model simplification, water sources
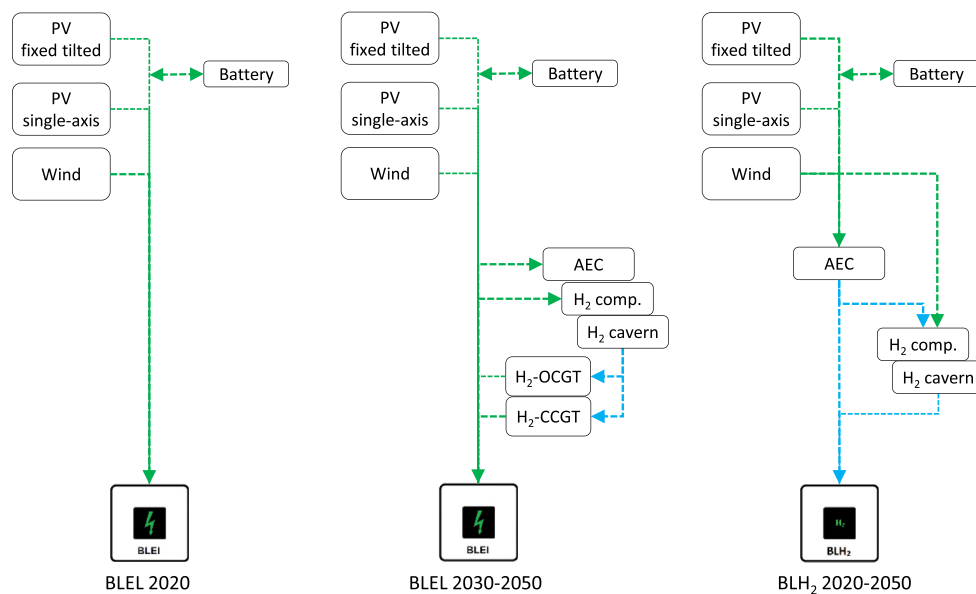

Fig. 1. BLEL (left, middle) and BLH$_2$ (right) *Onsite* model configurations. Commercially available hydrogen-fuelled gas turbines are assumed from 2030 onwards. Abbreviations: photovoltaic, *PV*, alkaline electrolyser, *AEC*, compressor, *comp.*, hydrogen-fuelled open cycle gas turbine, *H$_2$-OCGT*, hydrogen-fuelled combined cycle gas turbine, *H$_2$-CCGT*. Green and blue lines represent electricity and hydrogen flow, respectively. (For interpretation of the references to colour in this figure legend, the reader is referred to the Web version of this article.)
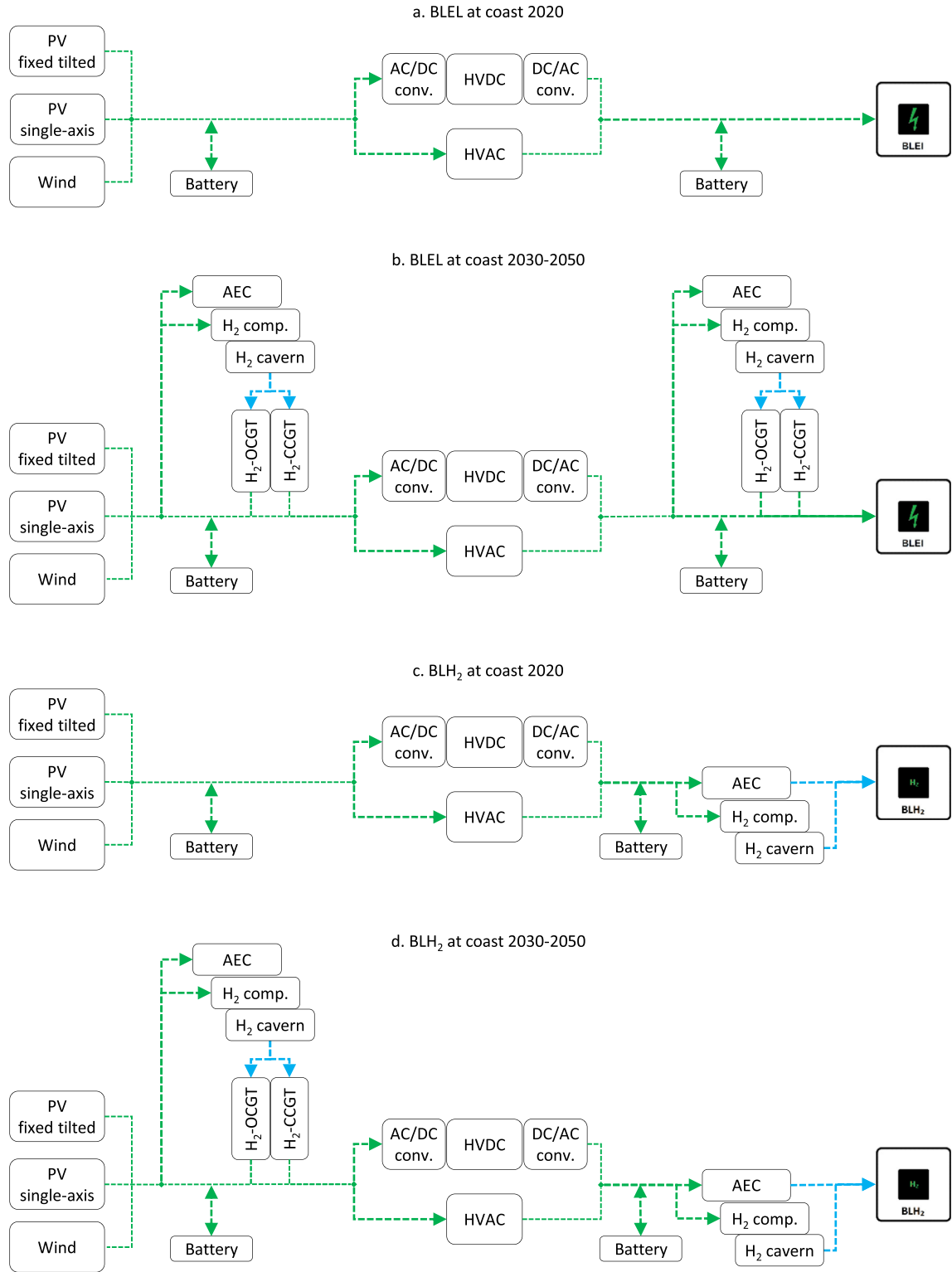
Fig. 2. BLEL (a, b) and BLH$_2$ (c, d) *Coastal* model configurations.

and their costs have been excluded from this study.

The equations below have been used to calculate the LCOE for power plants and the subsequent value chains, which follow respective guidelines published by the NREL (Short et al., 1995). Abbreviations: applied technology, *i*, capital expenditures, *Capex*, annual operational expenditures, *Opex*, full load hours per year, *FLh*,

fuel costs per unit of energy, *fuel*, efficiency of fuel converter, η, annuity factor, *crf*, weighted average cost of capital, *WACC*, lifetime, *N*. A weighted average cost of capital (WACC) of 7% is used for all the calculations in the base scenario. This is the real WACC (excluding inflation rate considered in nominal WACC, which is typically assumed to be around 2%). For the WACC of 7% in the base scenario,

assuming an equity share of 30% and an interest rate of 4%, this would lead to a return on equity of 14%.

$$\mathrm{crf} = \frac{\mathrm{WACC} \cdot (1 + \mathrm{WACC})^N}{(1 + \mathrm{WACC})^N - 1} \tag{1}$$

$$LCOE_i = \frac{Capex_i \cdot \mathrm{crf} + Opex_{i,fix}}{FLh_i} + Opex_{i,var} + \frac{\mathrm{fuel}}{\eta_i} \tag{2}$$

The model and its constraints are defined in the Matlab software, version R2016a (MathWorks, 2016). The defined constraints for the model, presented in Equation (3), ensure the hourly mass and energy balance of electricity generators (fixed tilted and single axis tracking PV, wind energy, H_2-OCGT, H_2-CCGT), electricity consumers (electrolyser, compressor, BLEL), battery charge and discharge, curtailed electricity, H_2 generator (electrolyser), H_2 consumers (compressor, H_2-OCGT, H_2-CCGT, BLH$_2$), cavern charge and discharge and electricity conversion and transmission technologies (AC/DC converter, HVAC, HVDC). Abbreviations: technology, *tech*, electricity, *El*, time, *t*, generation, *gen*, consumption, *cons*, battery, *Batt*, charge, *char*, discharge, *disch*, electricity curtailment, *curt*, transmission line, *TL*. Equation (3) is applied for both scenarios.

$$\forall h \in [1,\ 8760] \sum_t^{tech} El_{gen,t} - \sum_t^{tech} El_{cons,t} - Batt_{char,t} + Batt_{disch,t}$$
$$- El_{curt,t} + \sum_t^{tech} H2_{gen,t} - \sum_t^{tech} H2_{cons,t} - Cavern_{char,t}$$
$$+ Cavern_{disch,t} - \sum_t^{tech} TL_{in,t} + \sum_t^{tech} TL_{out,t}$$
$$= BLEL_t\ or\ BLH2_t$$
$$\tag{3}$$

A linear optimiser (Mosek, 2018) is used to achieve the hourly energy and mass balance throughout the year by combining applied technologies in a cost-optimal way, as presented in Equation (4). Abbreviations: installed capacity, *instCap*, generation, *Gen*.

$$\min\left(\sum_i^{tech} (CAPEX_i \cdot crf_i + OPEXfix_i) \cdot instCap_i + OPEXvar_i \cdot Gen_i\right)$$
$$\tag{4}$$

Average land use of 8.4 and 75 MW/km^2 is assumed for wind and PV power plants, respectively (Bogdanov and Breyer, 2016). In reality, PV installation rates per area at the equator are higher than those closer to poles, due to a lower shading effect. The world is divided into $0.45° \times 0.45°$ nodes, shaping a 400×800 matrix. As shown in Fig. 3, the maximum area is about 2500 km^2 for nodes at the equator, declining to less than 1200 km^2 at regions beyond $\pm 60°$ latitudes.

The model is allowed to use up to 10% of land at each node for PV (total of fixed tilted and single axis tracking) or wind power plant installations. First, the optimisations are done for relatively small-scale demands at each node and respective land use of installed PV and wind capacities are calculated. The system is then scaled up to the limit such that PV or wind energy land usage reaches its limit first, representing the generation potential of the cost-optimised configuration.

2.2. Data

The hourly solar irradiation and wind speed in a $0.45° \times 0.45°$ spatial resolution are taken from NASA databases (Stackhouse and
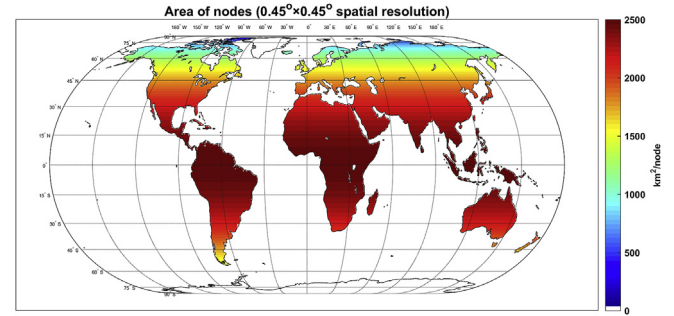
Fig. 3. Area of $0.45° \times 0.45°$ nodes.

Whitlock, 2008, 2009) and are partly reprocessed by the German Aerospace Centre (Stetter, 2012). Feed-in time series for fixed optimally tilted PV systems are calculated based on Gerlach et al. (2011) and Huld et al. (2008) to maximise the annual generation by considering the optimal PV module angle at each node, taking into account the irradiance angle, temperature and clouds impact on the hourly generation. Feed-in time series for single-axis tracking PV are based on Afanasyeva et al. (2018), which considers a horizontal north-south-orientated single-axis continuously tracking system and global horizontal irradiation (GHI), direct normal irradiation (DNI), other environmental conditions (e.g. ambient temperature), and PV system components, such as cabling, inverters, and transformers. Feed-in time series of wind power plants are calculated for ENERCON (2014) standard 3 MW wind turbines (E−101) with hub height conditions of 150 m, according to Gerlach et al. (2011).

All technical and financial specifications used in this study are provided in Table 1. An exchange rate of 1.35 USD/€ has been used for costs originally available in USD. The projected cost decline of PV and wind power plants as well as electrolysers and battery storage systems are based on projected deployment and learning rates of each technology as discussed in the respective references. Since gas turbines are already well developed and have been mass produced for decades, no capital cost decline is foreseen, but projected efficiency improvement is taken into account. According to Dana et al. (2016), higher efficiencies are achievable via H_2-CCGT than NG-CCGT, based on the fuels' higher heating value (HHV). However, considering the uncertainties with their costs, H_2-GTs are assumed to be available at NG-GTs efficiency and cost rates from 2030 onwards. The projected capex for HVDC and converter stations beyond 2040 are higher than earlier years due to the projected shift to higher voltage system with lower efficiency losses (Dii, 2014). As long distance HVDC lines might pass through populated areas with opposition to overhead power lines, it is assumed that 10% of the length of each HVDC line is built underground and blended specifications are calculated accordingly. The hydrogen storage system is based on man-made large salt caverns of about 500,000 m^3 of net storage volume, equal to about 156 GWh$_{H2,HHV}$ (Michalski et al., 2017).

3. Results

3.1. PV and wind FLh, their complementary role and LCOE

The FLh of a power plant is equivalent to hours of operation at full capacity to provide the same annual output. As such, the FLh of fixed tilted PV, single-axis tracking PV and wind power plants are shown is Fig. 4. The FLh of fixed tilted PV is more than 1300 FLh for most regions between $\pm 45°$ latitude, reaching 1800−1900 FLh in Tibet, Mexico, Namibia, South Africa and the MENA region, with a

Table 1
Technical and financial specifications.

Device		unit	2020	2030	2040	2050	reference
PV fixed tilted	capex	€/kW$_p$	580	390	300	246	ETIP-PV (2017)
	opex $_{fix}$	€/(kW$_p$·a)	13.2	10.6	8.8	7.4	
	lifetime	year	30	35	40	40	
PV single-axis tracking	capex	€/kW$_p$	638	429	330	271	ETIP-PV (2017); Bolinger et al. (2017)
	opex $_{fix}$	€/(kW$_p$·a)	15	12	10	8	
	lifetime	year	30	35	40	40	
Wind energy (onshore)	capex	€/kW$_p$	1150	1000	940	900	Neij (2008); Breyer et al. (2018)
	opex $_{fix}$	% of capex p.a.	2	2	2	2	
	lifetime	year	25	25	25	25	
Battery storage	capex	€/kWh	270	134	92	70	Breyer et al. (2018);
	opex $_{fix}$	€/(kWh·a)	9	3.75	2.5	1.875	Giuliano et al. (2016)
	opex $_{var}$	€/kWh	0.0002	0.0002	0.0002	0.0002	
	lifetime	year	20	20	20	20	
	cycle eff.	%	91	93	95	95	
	self-discharge	%/h	0	0	0	0	
Battery interface	capex	€/kW	135	67	46	35	Breyer et al. (2018);
	opex $_{fix}$	€/(kW·a)	all opex allocated to the storage part				Giuliano et al. (2016)
	lifetime	year	20	20	20	20	
Combined cycle gas turbine	capex	€/kW	-	775	775	775	EC (2014)
	opex $_{fix}$	% of capex p.a.	-	2.5	2.5	2.5	EC (2014)
	opex $_{var}$	€/kWh	-	0.002	0.002	0.002	EC (2014)
	lifetime	year	-	35	35	35	Farfan and Breyer (2017)
	eff. (LHV)	%	-	58	60	60	EC (2014); IEA (2016)
	eff. (HHV)	%	-	52.2	54	54	
Open cycle gas turbine	capex	€/kW	-	475	475	475	EC (2014)
	opex $_{fix}$	% of capex p.a.	-	3	3	3	EC (2014)
	opex $_{var}$	€/kWh	-	0.011	0.011	0.011	EC (2014)
	lifetime	year	-	35	35	35	Farfan and Breyer (2017)
	eff. (LHV)	%	-	43	44	45	EC (2014)
	eff. (HHV)	%	-	38.7	39.6	40.5	
HVDC (underground cable)	capex	€/(kW·km)	1.233 [1]	1.233 [1]	1.367 [2]	1.367 [2]	Dii (2014)
	opex $_{fix}$	% of capex p.a.	0.1	0.1	0.1	0.1	Dii (2014)
	lifetime	year	50	50	50	50	Bogdanov and Breyer (2016)
	efficiency	% per 1000 km	96.4 [1]	96.4 [1]	98.4 [2]	98.4 [2]	Dii (2014)
HVDC (overhead line)	capex	€/(kW·km)	0.20 [1]	0.20 [1]	0.30 [2]	0.30 [2]	Dii (2014)
	opex $_{fix}$	% of capex p.a.	1	1	1	1	Dii (2014)
	lifetime	year	50	50	50	50	Bogdanov and Breyer (2016)
	efficiency	% per 1000 km	93.4 [1]	93.4 [1]	98.4 [2]	98.4 [2]	Dii (2014)
HVDC (Blended)	capex	€/(kW·km)	0.303	0.303	0.407	0.407	this study:
	opex $_{fix}$	€/(kW·km·a)	0.0019	0.0019	0.0028	0.0028	10% underground and 90% overhead
	lifetime	year	50	50	50	50	Dii (2014)
	efficiency	% per 1000 km	93.5	93.5	98.4	98.4	Dii (2014)
HVAC [3] (overhead line)	capex	€/(kW·km)	0.244	0.244	0.244	0.244	Dii (2014)
	opex $_{fix}$	% of capex p.a.	1	1	1	1	Dii (2014)
	lifetime	year	50	50	50	50	Bogdanov and Breyer (2016)
	efficiency	% per 1000 km	86	86	86	86	Dii (2014)
Converter station	capex	€/kW	150 [1]	150 [1]	180 [2]	180 [2]	Dii (2014)
	opex $_{fix}$	% of capex p.a.	1	1	1	1	Dii (2014)
	lifetime	year	50	50	50	50	Dii (2014)
	efficiency	%	98.6	98.6	98.6	98.6	Dii (2014)
Alkaline water electrolyser (40 bar outlet)	capex	€/kW$_{H2,HHV}$	685	380	296	248	Agora Energiewende (2014);
	opex $_{fix}$	% of capex p.a.	0.035	0.035	0.035	0.035	ETOGAS GmbH (2013);
	opex $_{var}$	€/kWh$_{H2}$	0.0012	0.0012	0.0012	0.0012	2040 and 2050 based on learning curve
	lifetime	year	30	30	30	30	
	eff. (HHV)	%	82.3	82.3	82.3	82.3	
H$_2$ compressor	capex	€/kW$_{H2,HHV}$	256	256	256	256	Michalski et al. (2017)
	opex $_{fix}$	% of capex p.a.	4	4	4	4	Michalski et al. (2017)
	lifetime	year	15	15	15	15	Michalski et al. (2017)
	pressure range	bar	40-200	40-200	40-200	40-200	Michalski et al. (2017)
	el. consumption	kWh$_{el}$/kWh$_{H2,HHV}$	0.02 [3]	0.02 [3]	0.02 [3]	0.02 [3]	Makridis (2016)
H$_2$ seasonal storage (man-made salt cavern)	capex	€/kWh$_{H2,HHV}$	0.24	0.24	0.24	0.24	Michalski et al. (2017)
	opex $_{fix}$	% of capex p.a.	3	3	3	3	
	lifetime	year	30	30	30	30	Michalski et al. (2017)
	cycle eff.	%	100	100	100	100	
	pressure range	bar	60-200	60-200	60-200	60-200	Michalski et al. (2017)

[1] 500 kV.
[2] 800 kV.
[3] Isothermal.

maximum in the Atacama Desert at about 2200 FLh. Single-axis tracking PV increases PV FLh by up to 30% in comparison to fixed tilted PV, particularly in Eastern Brazil, Horn of Africa, Central Africa, South of Saudi Arabia, Northeast Australia and at latitudes above 70°N. As such, single-axis tracking PV FLh reaches about 2000−2400 h in the northern half of Australia, Africa, Middle East, Tibet, Mexico, Eastern Brazil, with the Atacama Desert as the best site at about 2500 FLh. On the other hand, wind power plant FLh range is relatively higher in many regions, where best sites reach around 4500−6500 FLh in Patagonia, Tibet, near Beijing, Horn of Africa, Central US, Newfoundland and Labrador in Canada, Iceland, Ireland, UK and the coastal line of Western Europe and Australia. The applied 93% wind power plant disturbance factor stands for wake effects on wind quality reaching downstream turbines in a wind farm, in comparison to a single wind turbine, and also includes the availability of the wind power plant.

The first step in achieving higher FLh towards baseload electricity from PV and wind energy is to understand the potential of these RE sources. The FLh of PV and wind power plants is typically reported based on the nominal capacity of panels or turbines. However, provided FLh for demand coverage should be calculated based on the demand capacity, which could be sized to the generators' maximum real output capacity or less. For example, Afanasyeva et al. (2018) and Giuliano et al. (2016) oversize the dimensions of PV modules to inverter capacity by 129%, as a global average for optimising the trade-off between yield and capex. Considering losses in cables and transformers, the studied single-axis tracking PV power plants' hourly output power is never more than 75.5% of its PV modules' nominal capacity. Thus, electricity uptake with a capacity of 75.5% of PV modules' nominal capacity could still consume all the output energy from the PV power plant, leading to 32.5% increase in FLh from the electricity uptake perspective (Fig. 5), with no extra curtailment or storage (Equation (5)). Adjusting the electricity uptake capacity to the wind power plant maximum outlet capacity would deliver a 7.5% higher FLh to the electricity uptake.

$$Annual\ el.\ generation = Capacity_{PV\ modules}$$
$$\times FLh_{PV} \approx Capacity_{uptaking} \times FLh_{uptaking} \qquad (5)$$

Combining different sources of renewable electricity, namely PV and wind energy in this study, can increase the overall availability of electricity for baseload demand. Fig. 6 illustrates the complementary impact of single-axis tracking PV and wind energy for equal nominal installed capacities of PV, wind energy and electricity demand during 200 h in a random node. The overall electricity generation could exceed the demand at hours with both good PV and wind electricity generation, which would be curtailed in the absence of electricity storage. Such extra production is defined as critical overlap (Gerlach et al., 2011) and its respective FLh is defined as curtailed generation based on the uptake capacity, which is calculated via Equation (6). The index "rp" stands for hourly rated power in relation to nominal capacity of respective generators.

$$Critical\ overlap\ FLh = \sum_{t=1}^{8760} max\big([PV_{rp}(t) + Wind_{rp}(t) - 1], 0\big)$$
$$(6)$$

The global maps for critical overlap FLh and cumulative FLh adjusted by critical overlap for hybrid fixed tilted PV-wind and hybrid single-axis tracking PV-wind power plants are shown in Fig. 7. In most parts of the world, the critical overlap is below 500 h, with the exception of Patagonia, the Atacama Desert, the Horn of Africa and Tibet, due to their extremely good wind conditions during daytime. In addition to these regions, the cumulative hybrid PV-wind FLh (critical overlap excluded) at the joint border between Libya, Niger and Chad exceeds 6000 h, representing high levels of solar and wind compatibility at very low critical overlaps. However, nowhere in the world does the cumulative hybrid PV-wind FLh exceed 6500 and is thus unable to provide baseload electricity.

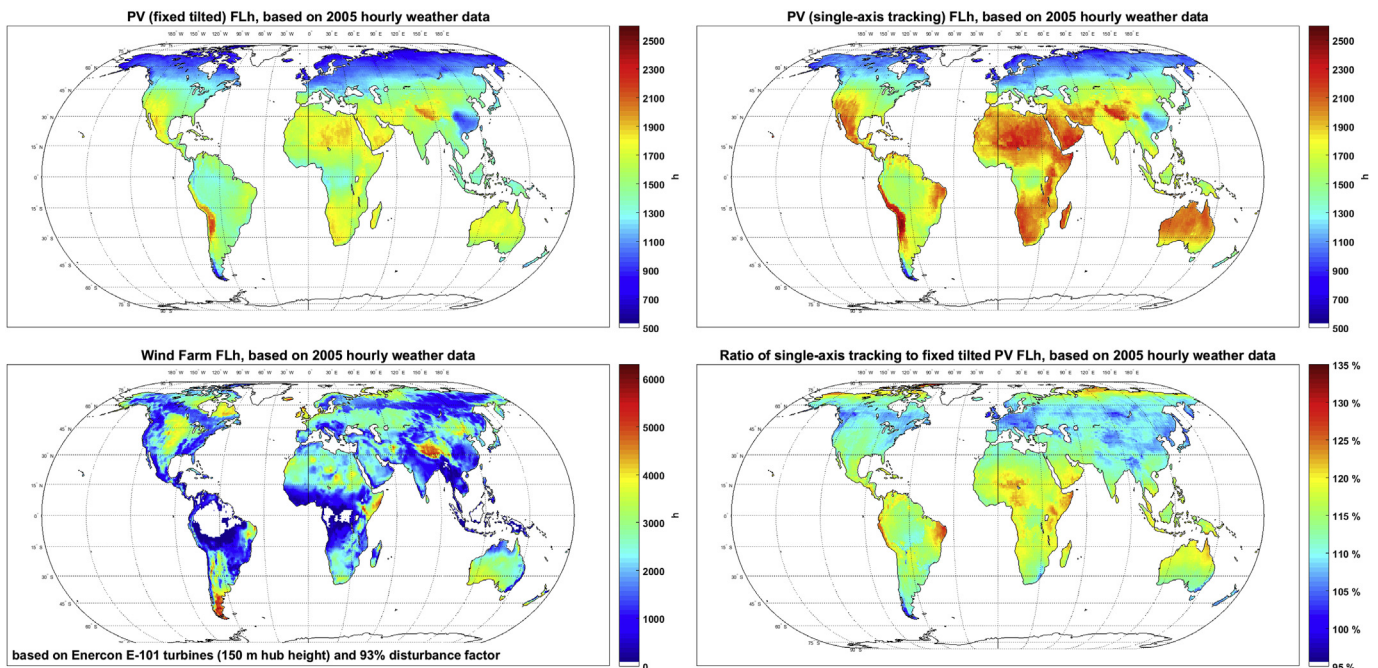Combining equal actual output capacities of single-axis tracking

Fig. 4. Full load hours of PV fixed tilted (top left), PV single-axis tracking (top right), wind energy (bottom left) and ratio of single-axis tracking to fixed tilted PV FLh (bottom right) for 2005 weather data.
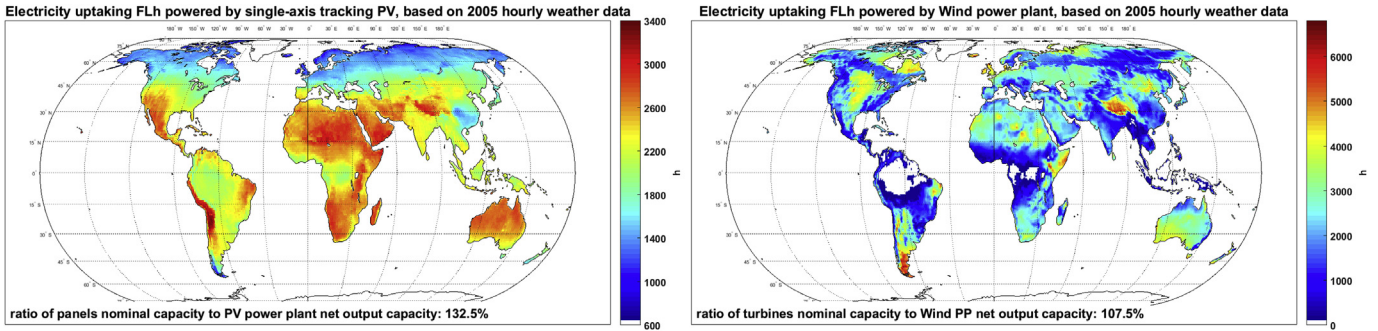
Fig. 5. Full load hours of PV single-axis tracking and wind power plants for 2005 weather data, from the perspective of electricity uptake.
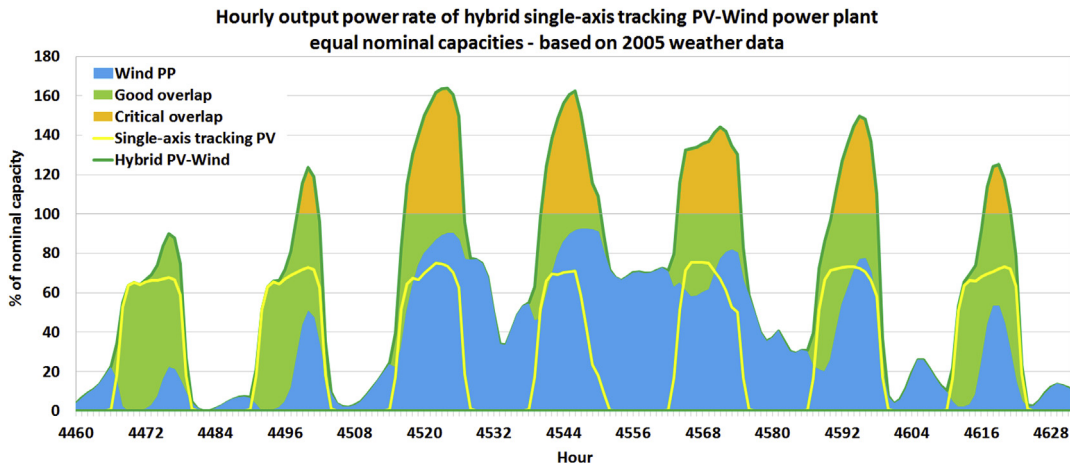

Fig. 6. Sample for complementary impact of solar PV and wind energy for increasing power FLh.
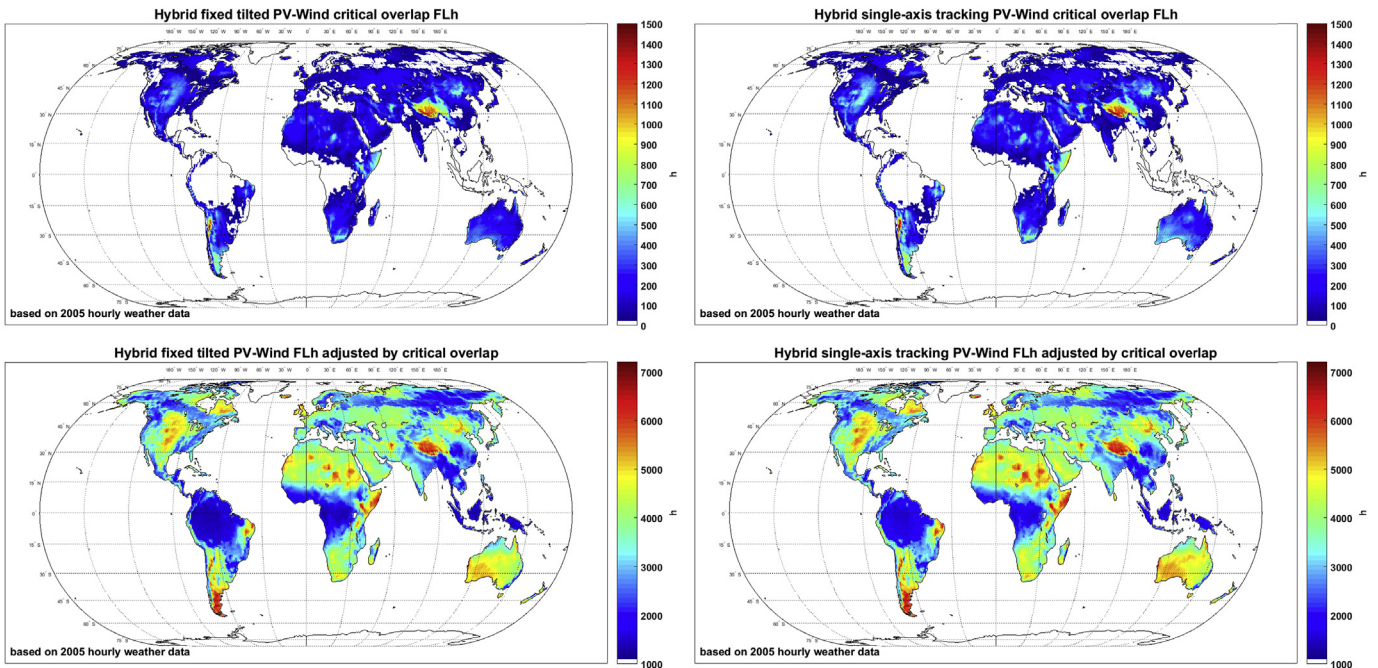

Fig. 7. Critical overlap full load hours of fixed tilted PV-wind (top left), single-axis tracking PV-wind (top right), adjusted cumulative FLh of fixed tilted PV-wind (bottom left) and single-axis tracking PV-wind (bottom left) for 2005 weather data.

PV and wind power plants (132.5% PV and 107.5% wind nominal capacities) would lead to higher cumulative FLh, shown in Fig. 8. However, nowhere can it reach 8760 FLh from an electricity uptake perspective. In addition, this cumulative FLh only indicates a physical feasibility of increasing electricity availability by installing equal capacities of PV and wind energy, while a cost-optimised solution would be based on different shares of PV and wind energy and electricity storage options depending on the electricity generation profiles of each region and the respective cost assumptions of the technologies.

The LCOE of independent fixed tilted and single-axis tracking PV power plants are illustrated in Fig. 9. The LCOE is a function of FLh and financial assumptions in a way that regions with higher FLh generate lower cost electricity. For fixed tilted PV, the LCOE at the best sites drops from about 30 €/MWh in 2020 to about 15 €/MWh in 2050. Although the capital and operational expenditures of single-axis tracking PV are higher than fixed tilted PV, single-axis tracking PV generates lower cost electricity in regions with relatively higher FLh. Besides LCOE, the electricity generation profile for fixed tilted and single-axis tracking PV differs around the globe throughout the year, which would have an impact on the complementing role of PV to wind energy or battery storage and the electricity curtailment level of hybrid systems in relation to the demand capacity.

As can be seen in Fig. 10, wind energy LCOE is more location dependent and shows greater variation. In 2020, wind energy LCOE of about 30 €/MWh is achievable in Northeast Canada, central US, Southern America, UK, and the Western coast of Europe, Northern Africa, Horn of Africa, Tibet and Mongolia. The least wind energy LCOE, which is in Patagonia, declines from about 25 to 15 €/MWh, from 2020 to 2050, respectively. In general, the projected cost reductions for wind energy are lower than those for PV systems.

3.2. Levelised costs of BLEL and BLH$_2$

The levelised cost of baseload electricity (LCOBLEL) in the cost-optimised configurations for the *Onsite* and *Coastal Scenarios* for the years 2020−2050 in 10-year steps are illustrated in Fig. 11. For the 2020 scenario, LCOBLEL at latitudes above 55°N is more than 300 €/MWh, which is significantly higher than for the 2030 scenario. The reason for the high LCOBLEL is that in higher latitudes the wind FLh is not particularly high and solar PV has strong seasonality. In the absence of a PtH$_2$tP solution for the 2020 scenario, several days of no significant wind energy in the darkest days of the year would lead to over-dimensioning of power generators and additional battery storage installations. Nevertheless, in 2020, LCOBLEL of 100−130 €/MWh is achievable onsite in the Atacama Desert, the MENA region, the Horn of Africa and Tibet. By introducing PtH$_2$tP to the model in 2030, along with the cost decline of RE technologies, a

significant decline in the LCOBLEL is achieved. In 2030, best sites in the world, namely Patagonia and Tibet, could deliver BLEL at costs below 50 €/MWh. In 2050, costs below 40 €//MWh are achievable in most regions of Africa, the Middle East, Central Asia, Australia, Southern US, Mexico and Central and Southern America. The lowest-cost sites in 2050 are at a cost level of around 31 to 34 €/MWh and can be found in the Atacama Desert, Niger, Chad, South of Libya, Somalia, Yemen and Oman. For the *Coastal Scenario*, the cost of electricity from remote areas delivered to the coast is relatively higher, depending on the distance and the year. In 2050, this impact is reduced by lower cost electricity and lower losses in the transmission lines.

For baseload hydrogen, as shown in Fig. 12, lower costs are achievable in 2020 and 2030 in comparison to BLEL, due to the flexibility of electrolysers and the availability of relatively low-cost hydrogen storage in comparison to long-term electricity storage. As such, regions with excellent wind resources, such as Patagonia, would be attractive for delivering low cost BLH$_2$ even in 2020. By 2050, BLH$_2$ could be produced at costs below 40 €/MWh$_{H2,HHV}$ (1.58 €/kg$_{H2}$) on all continents. However, for the *Coastal Scenarios*, nodes close to the coast would be more attractive, avoiding the cost of transmission lines.

3.3. Technology and cost analysis (sample nodes)

To provide a deeper understanding of the model, the installed capacities, generation or consumption of relevant components for 3 nodes from all the four scenarios in 2030 are provided in this section. The chosen nodes are based on the following criteria:

- 53.0 €/MWh$_{H2,HHV}$ < LCOBLH$_2$ < 53.5 €/MWh$_{H2,HHV}$
- 700 km < distance to coast <1000 km

And represent different mixes of power generation technologies in the *Onsite BLH$_2$ Scenario*:

- Node 1: PV-based system: 22.9 °S, 136.8 °E, Australia
- Node 2: wind-based system: 52.65 °N, 97.2 °W, Canada
- Node 3: mixed system: 27.45 °S, 62.1 °W, Argentina

Fig. 13 illustrates the installed capacities for 1 GW$_{th}$ baseload hydrogen (HHV) at the defined nodes. More than 5 GW of single-axis tracking PV is needed to provide 1 GW$_{th}$ of BLH$_2$ in the PV-dominated system of node 1. Wind installations increase in all nodes for the *Coastal Scenario* in comparison to the *Onsite Scenario*, as higher wind FLh is desired to reduce the transmission line costs by increasing its rate of utilisation. In addition, higher installed capacities are needed to compensate for the transmission line costs. Node 3 with mixed technologies provides the most stable power profile, which leads to the lowest electrolyser and compressor capacities. Compressor capacities are 1 GW$_{th}$ lower than electrolyser capacities, as the first 1 GW$_{th}$ of hydrogen is directly used and is not compressed into the cavern. The hydrogen state of charge in nodes 1, 2 and 3 is illustrated in Figure S1.

Relatively high FLh of PV-based electrolysers are observed with no battery installation. Based on detailed installed capacities and annual energy flows in Tables S1 and S2, the 1 GW$_{H2,HHV}$ *Onsite* BLH$_2$ system in node 1 is solely powered by 5.55 GW$_p$ of solar PV systems (with about 95% single-axis tracking PV), with hybrid FLh of 2065 h. Meanwhile, electrolysers have FLh of 3070 h, because FLh of PV systems is based on the PV panels' nominal capacity, while the electrolysers' capacity is optimised according to the power plants' output power (Fig. S2). In node 1, electrolysers' power uptake capacity of 3.46 GW$_p$ (2.85 GW$_{H2,HHV}$) is 62% of the PV plants' nominal capacity, which results in about 49% higher FLh for
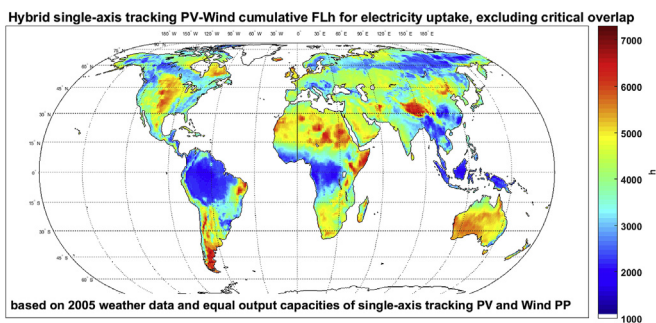

Fig. 8. Hybrid single-axis tracking PV-wind cumulative FLh for electricity uptake, excluding critical overlap, for 2005 weather data.
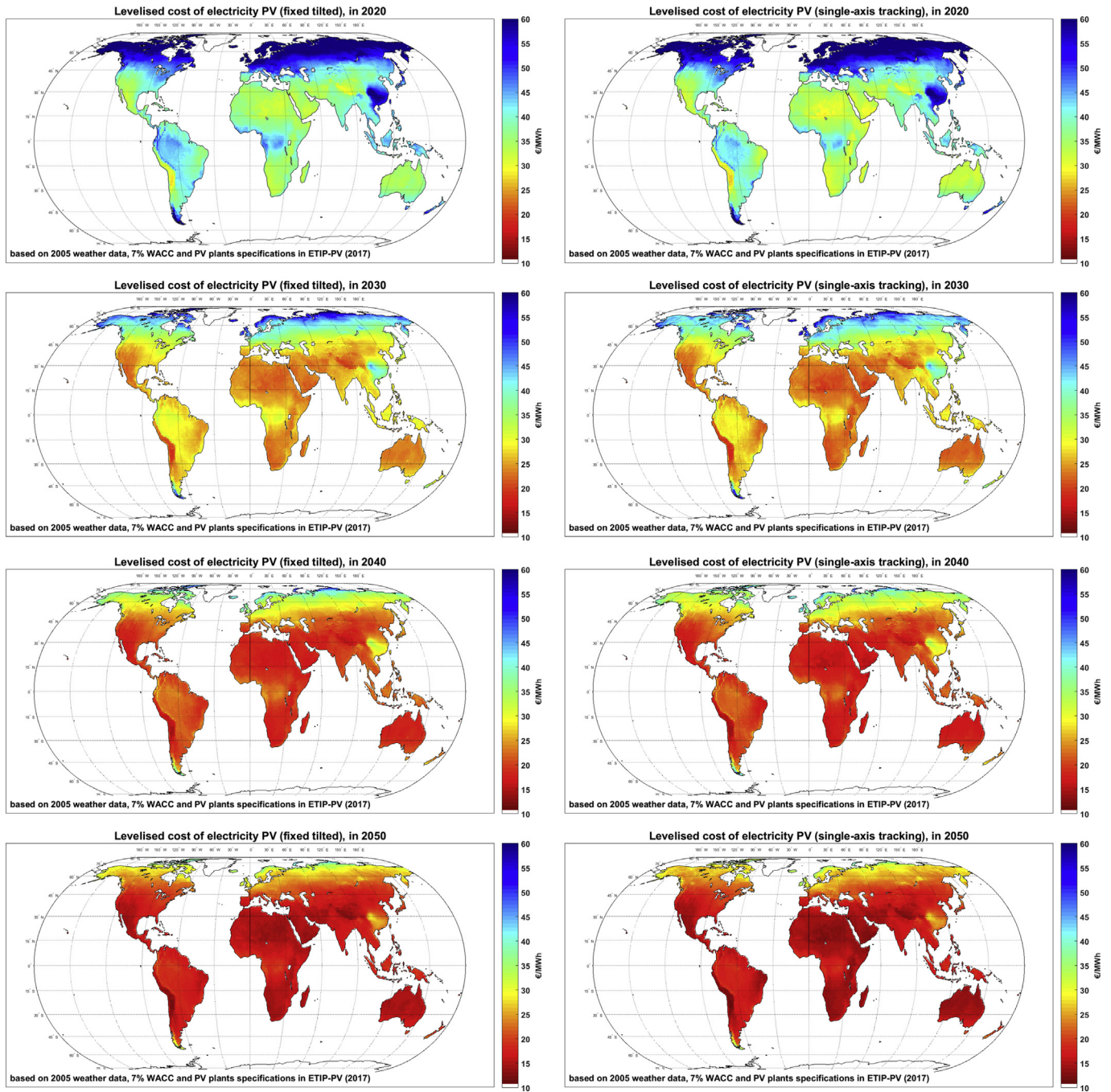
Fig. 9. Levelised cost of PV fixed tilted (left) and single-axis tracking (right) for 2020 (top), 2030 (upper centre), 2040 (lower centre) and 2050 (bottom).

electrolysers in comparison to PV power plants. At this electrolyser capacity, 0.9% of total generated electricity is consumed by the compressor and 6.3% is curtailed, which is part of the cost-optimised configuration.

The cost-optimised configuration for BLEL at the same nodes is significantly different from that for BLH_2, as shown in Fig. 14. Due to higher costs of electricity balancing technologies, a more steady electricity generation profile is important and all three nodes see a mix of both PV and wind energy technologies. Unlike the BLH_2 scenario, the capacities of electrolysers and compressors are equal, as all the generated hydrogen needs to be stored before consumption in GTs. H_2-CCGT has the highest balancing power

capacity in all the nodes, followed by battery power and H_2-OCGT. For *Coastal* BLEL, the systems are mainly balanced before the transmission lines and HVDC is used to minimise the losses of relatively expensive balanced electricity.

Detailed installed capacities and annual energy flows of all discussed scenarios and nodes are provided in Tables S1 and S2 of the supplementary material.

The annualised cost of the system for the three studied nodes in all four scenarios are illustrated in Fig. 15. The annualised costs are even for BLH_2 *Onsite* for all three nodes, as they have been chosen to have very similar final costs. However, the composition of technologies is different. In none of the three nodes is battery storage
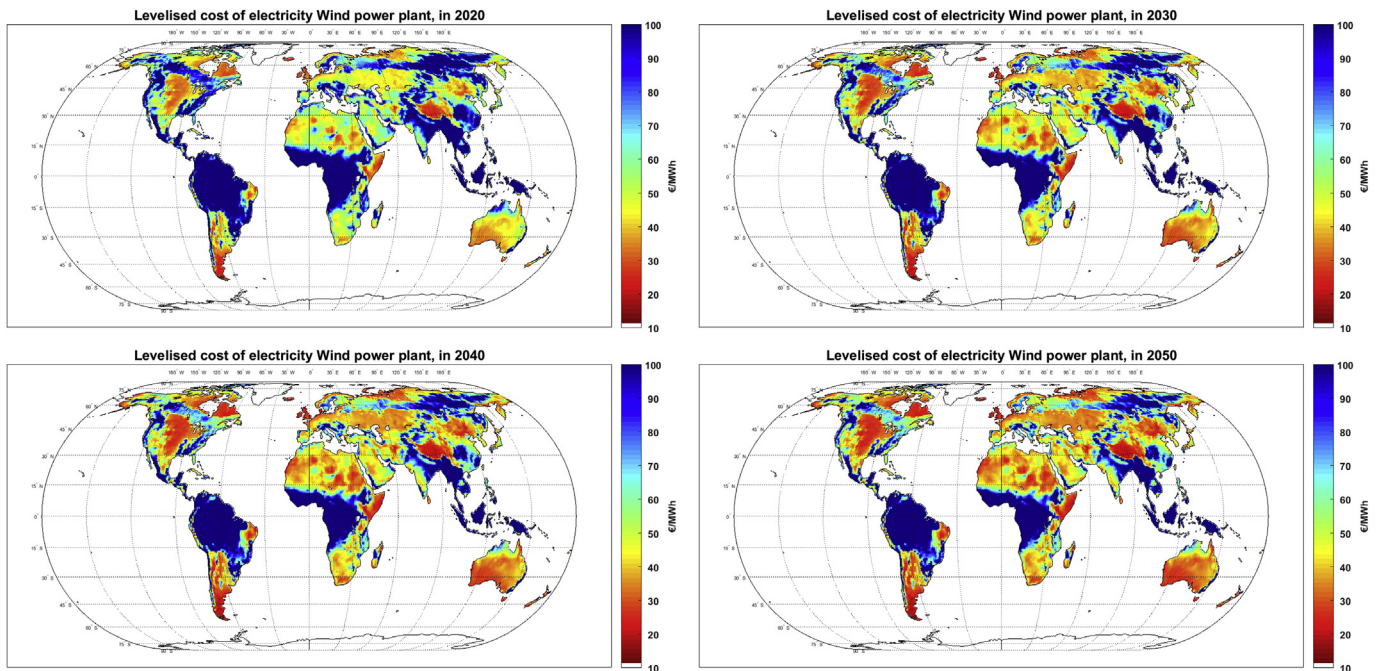
Fig. 10. Levelised cost of wind electricity (3 MW wind turbines, 150 m hub-height, power plant configuration) for 2020 (top left), 2030 (top right), 2040 (bottom left) and 2050 (bottom right).

installed to increase the system FLh. In node 1, the annualised cost of the hydrogen compressor is about three times more than its cost in node 3, due to larger demand for compressors to match the daily fluctuation of PV solar power.

For *Coastal* BLH$_2$, node 1 has a slightly higher annualised cost, despite the distance of node 1 to the coast being shorter than node 3, because the PV-dominated node 1 would provide electricity at lower FLh, leading to a lower utilisation rate of transmission lines and consequently higher costs. To minimise this impact, the cost-optimised solution for node 1 in the *Coastal Scenario* is achieved by installing some wind in the mix, which increases the FLh of electricity delivered to the transmission lines and reduces the required capacity of transmission lines, electrolysers and compressors. On the other hand, more wind in the mix increases the electricity generation costs. Battery installations could have been the other option for increasing the FLh of inlet electricity to the transmission lines. However, the PV and wind combination is a cheaper solution in this case. Table S3 provides detailed information of the data used in Fig. 15 for further analyses.

The hourly supply of electricity for BLEL *Onsite* for node 1 in 2030 is illustrated in Fig. 16. PV has the dominating installed capacity in this node (Tab. S1), which is clearly visible in the peaks of the hybrid PV-wind generation profile, while a share of baseload power is still provided by wind power plants at night-time within the illustrated hours. Batteries and H$_2$-CCGT are part of the daily mix providing baseload electricity, while H$_2$-OCGT is operational at peak demand hours every few days. The hourly electricity supply of battery storage and gas turbines for the whole year are provided in Figure S3.

While batteries and GTs are mainly operational during hybrid PV-wind power deficit hours, the total power output of hybrid PV-wind-battery-GTs at specific hours is more than BLEL demand (blue guide arrows on Fig. 16). Regardless of efficiency losses, this extra generation by balancing plants marks an electricity interchange between batteries and PtH$_2$tP systems, illustrated in Fig. 17. When the balancing electricity demand until the next battery charge

opportunity is less than the electricity stored in the battery (about hour 4265), the extra available stored electricity in the battery can be used to run the electrolyser during the deficit of RE to decrease the costs of hydrogen generation by increasing electrolyser operating hours, and also to avoid solar PV curtailment on the following day, in the case of fully charged batteries and electrolysers operating at full capacity. This electricity interexchange is known as the battery-to-power-to-gas effect and is described in more detail in Gulagi et al. (2018). On the other hand, the storage capacity of the batteries would not be significant for long periods with low direct electricity generation. At such hours, operation of the installed CCGT is the next balancing solution due to its higher efficiency. Later, the relatively cheaper OCGT installed capacity comes into operation to meet the peak demand, while its lower efficiency would not be that decisive, as the operating time is shorter. However, at 0.61 GW, the overall installed capacity of CCGT and OCGT in node 1 is less than the baseload demand, which makes it impossible for the balancing system to meet the full baseload demand in the absence of battery power. Thus, during long periods with power generation below the baseload demand level, GTs stay fully operational even at hours when the electricity deficit is less than the GTs' total capacity (about hour 4010), which gives the battery storage the possibility to partly recharge (see battery state of charge in Figure S4) and be available to meet the gap between GTs' capacity and the required balancing capacity in the upcoming hours with direct electricity deficit. Although the power-to-hydrogen-to-power-to-battery-to-power route has higher efficiency losses, its operation for limited hours is part of the cost-optimised solution to avoid the need for additional battery or GT installation to meet peaks in demand.

As illustrated in Fig. 18, for BLEL at the coast from node 1, the main part of balancing happens before the transmission line. The transmission line consists of mainly HVDC that runs on baseload at most hours of the year, except some limited hours with severe lack of energy. At such hours, H$_2$-OCGT plays the role of filling the gap. The electricity for the electrolyser after the transmission line is
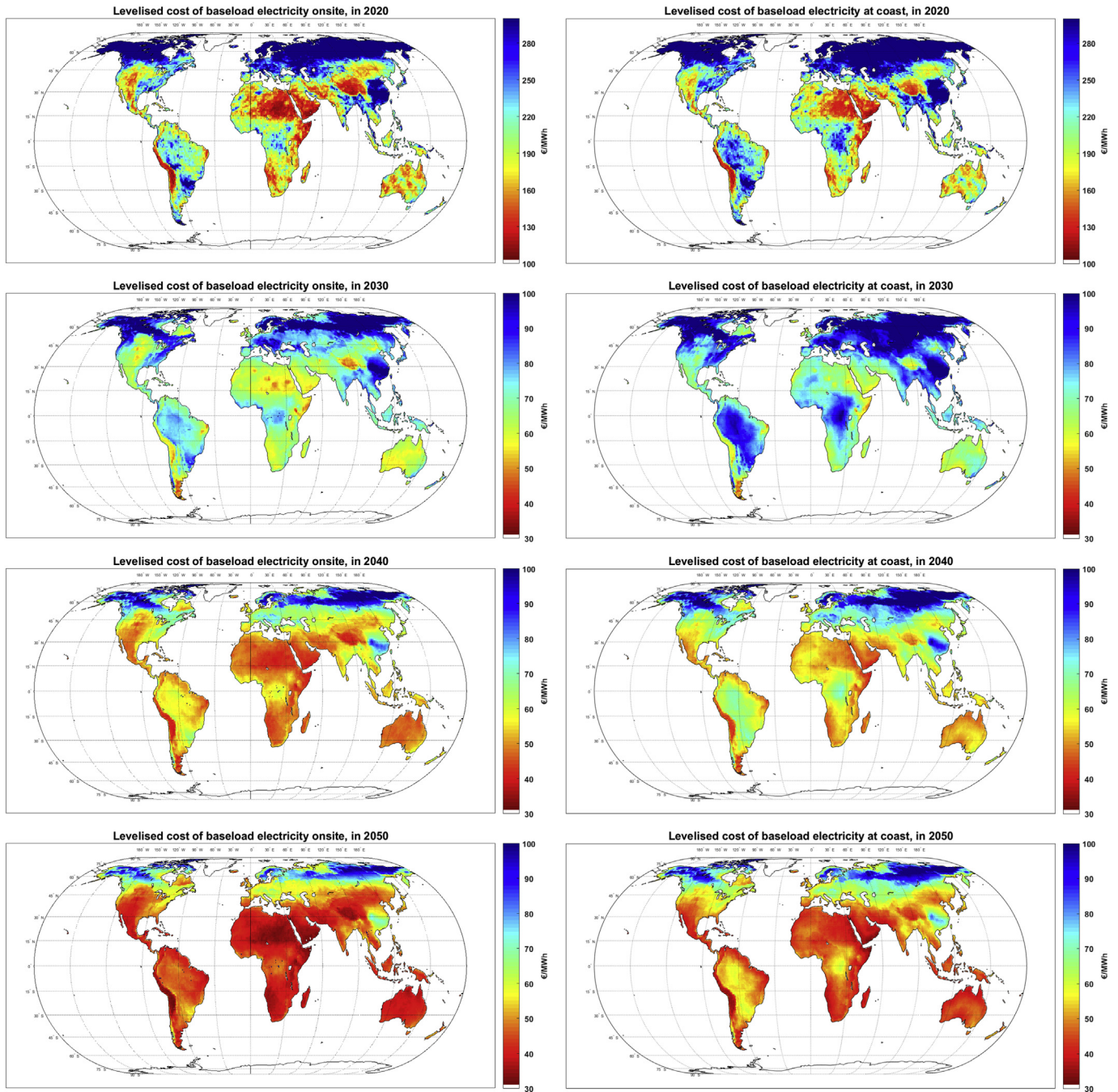
Fig. 11. Levelised cost of baseload electricity *Onsite* (left) and *Coastal* (right) for 2020 (top), 2030 (upper centre), 2040 (lower centre) and 2050 (bottom).

provided by HVAC lines transmitting the peak electricity at lower costs.

3.4. Technology mix and cost analysis for global trends

The global results for 2030 and 2050 are provided and analysed in this section for a better understanding of the global variation of each component in a cost-optimised system based on local conditions and change in technical and cost assumptions within the defined time frame. Figures for 2020 and 2040 are available in the Supplementary Material (Figures S5-S18).

As shown in Fig. 19, there is a general shift towards higher shares of solar PV from 2020 to 2050 for both BLEL and BLH$_2$ systems, due

to sharper cost declines of solar PV and battery in comparison to wind energy. However, at each specific year, the difference in PV share of BLEL and BLH$_2$ systems does not follow a general pattern and is location dependent. As hydrogen storage is relatively cheap, the daily or seasonal electricity variability is of less importance and the role of battery storage is not significant for smoothing hydrogen generation for BLH$_2$ (Fig. 21). Thus, the shares of PV and wind are mainly derived by the costs and FLh of the hybrid electricity for cheap hydrogen generation and the relatively minor costs of curtailment and extra hydrogen compression and storage. On the other hand, a different mix of PV and wind can shape the cost-optimised solution for the BLEL systems, depending not only on their FLh and costs, but also the hourly complementary role of PV
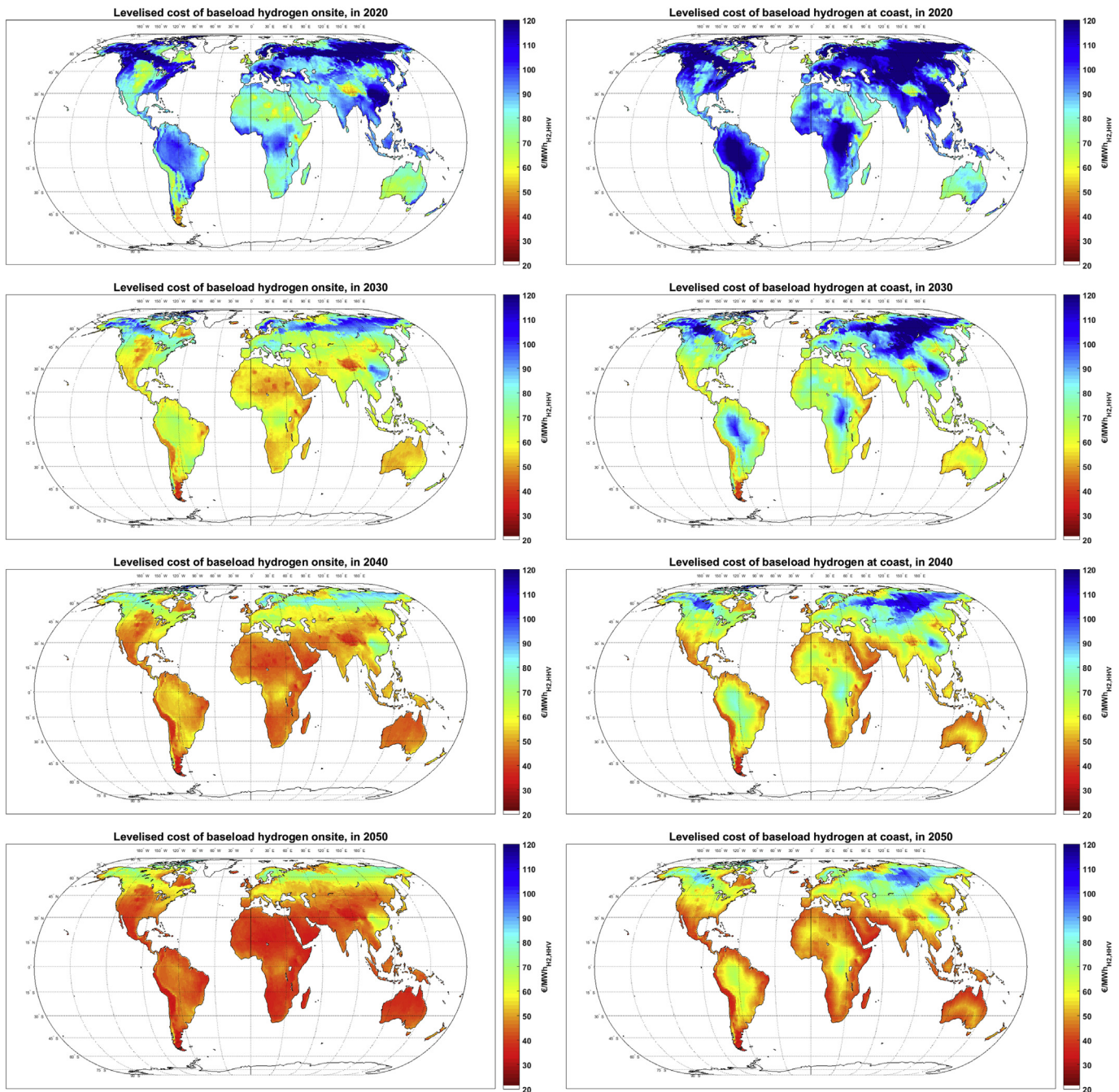
Fig. 12. Levelised cost of baseload hydrogen *Onsite* (left) and *Coastal* (right) for 2020 (top), 2030 (upper centre), 2040 (lower centre) and 2050 (bottom).

and wind energy and the compatibility of the hybrid generation with available storage options, namely batteries and PtH_2tP systems. For instance, central US has relatively good wind resources and solar conditions are best in the southwestern US (Fig. 4), which leads to mixed and PV-dominated BLH_2 systems in the central and the southwestern US, respectively. However, the PV-dominated nodes see more wind in the mix for BLEL as a balancing solution, while the central US nodes see a shift towards less wind in the mix of resources for BLEL for the same balancing. Nevertheless, many PV-dominated nodes for BLH_2, such as those in $15°S-15°N$ latitude, remain PV-dominated in BLEL systems as they can be effectively balanced with battery storage. In 2050, the PV-dominated nodes for BLH_2 see lower rise in wind power shares in BLEL systems in

comparison to 2030, due to sharper cost declines of battery and PtH_2tP systems as the balancing solution in comparison to wind energy.

Trieb et al. (2006) report a HVDC to HVAC breakeven distance of between 500 and 1000 km, based on the investment costs, for the interconnection of the MENA region and Europe. However, in addition to the capex of the transmission lines, the cost-optimised solution also depends on the LCOE and FLh of input electricity, efficiency of the transmission lines and the distance. As shown in Fig. 20, for BLEL, HVAC is chosen for distances less than about 500 km and a rather sharp shift towards HVDC is observed for longer distances, because electricity is mainly balanced before the transmission line and the higher losses of HVAC at long distances

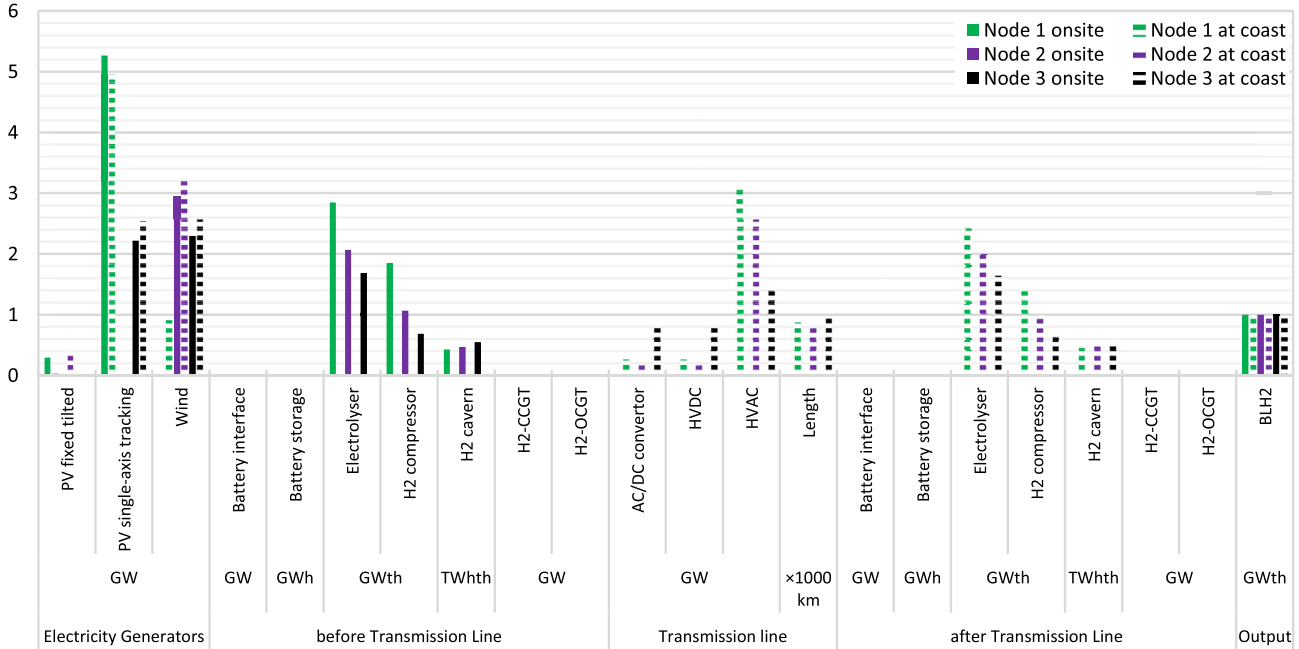Installed capacites for 1 GW$_{th,HHV}$ baseload hydrogen onsite and at coast for 3 sample nodes in 2030

Fig. 13. Mix of technologies for 1 GW$_{H2,HHV}$ BLH$_2$ *Onsite* and *Coastal* in 2030.

Installed capacites for 1 GW baseload electricity onsite and at coast for 3 sample nodes in 2030
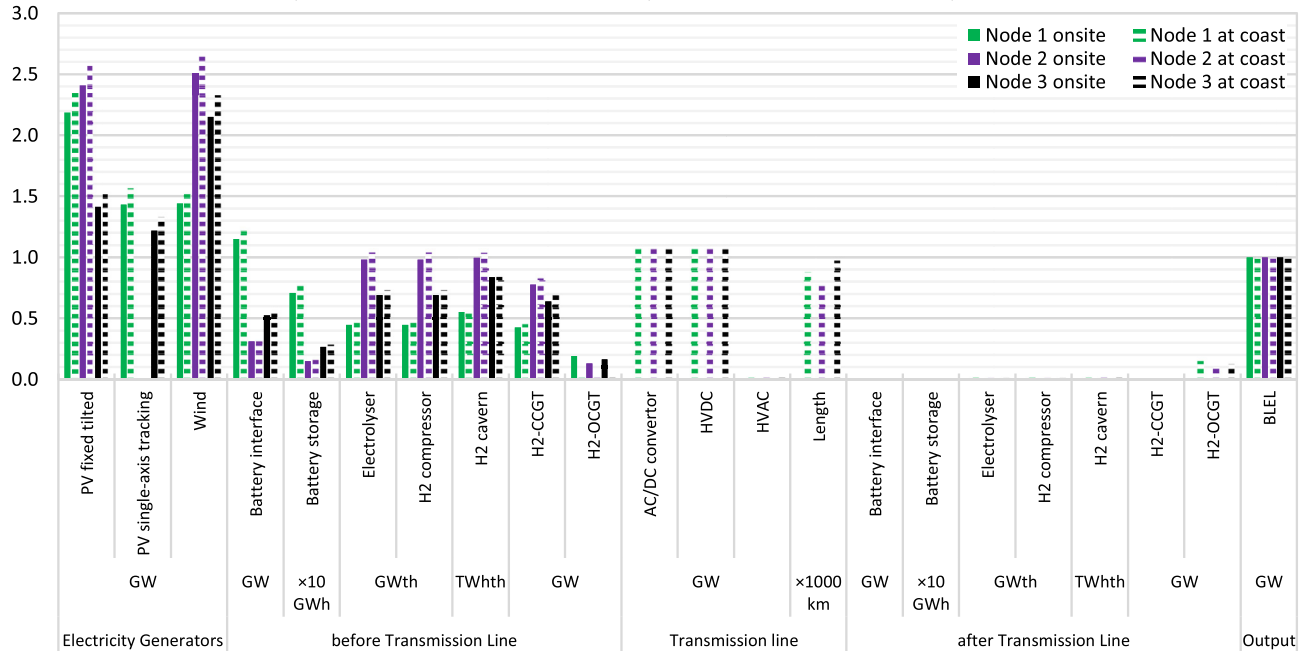

Fig. 14. Mix of technologies for 1 GW BLEL *Onsite* and *Coastal* in 2030.

would be costly. On the other hand, for BLH$_2$ in 2030, HVAC-dominated distance is up to 1000 km, because the power uptake by electrolysers is flexible and, for longer distances, the transmission of low-cost variable electricity via higher capacities of relatively cheaper HVAC at higher losses is cheaper than investment in more electricity balancing technologies before the more expensive and efficient HVDC transmission lines. Smaller shares of HVAC are still part of the system at distances beyond 1000 km for

electricity transmission at peak hours with low FLh.

Further, the cost decline rate of the battery component from 2030 to 2050 is the highest among all applied technologies, while the HVDC applied in 2050 has a higher capital expenditure in a trade-off with lower losses. These financial and efficiency changes lead to installation of more battery power in the cost-optimised systems in many regions to increase the utilisation rate of more expensive HVDC, and, to a lesser extent, HVAC. As a consequence,
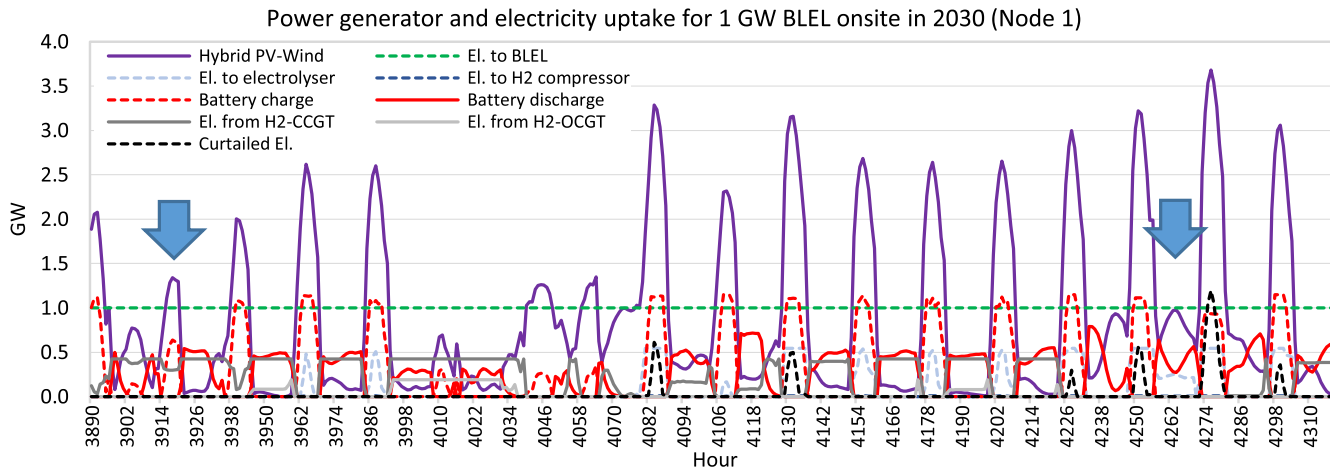
Fig. 15. Annualised costs of 1 GW baseload electricity and 1 GW$_{H2,HHV}$ baseload hydrogen by subcomponents for 3 sample nodes, in *Onsite* and *Coastal Scenarios* in 2030.

Fig. 16. Hourly supply of electricity by technology for BLEL *Onsite* for node 1 in 2030.

the total transmission line installed capacity decreases in remote areas. In addition, HVDC transmission lines are about 5% more efficient in 2050 and more suitable for power transmission at high FLh, which leads to less HVAC in the BLH$_2$ case. In comparison to BLH$_2$ in 2030, the more efficient HVDC line in 2050 has the biggest

impact on the share of HVDC at the switching distance from HVAC to HVDC, where the share of HVDC increases significantly in 2050. Such a pattern is not observed in regions above 60°N as battery storage would still not be a part of the cost-optimised solution. The same pattern is seen in central Australia, in which the battery

Fig. 17. Hourly power generator and electricity uptake for 1 GW BLEL *Onsite*, in 2030 (node 1).
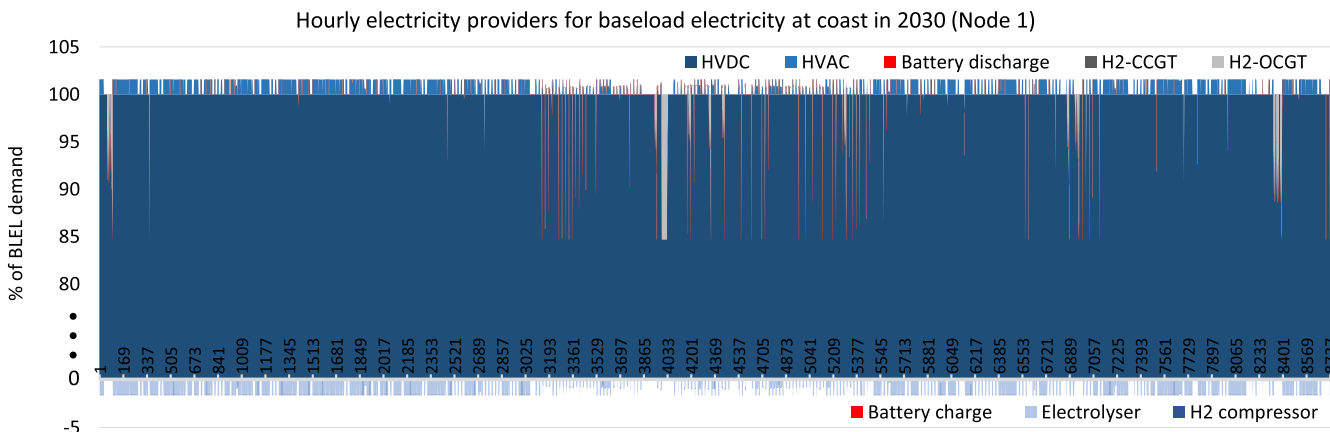
Fig. 18. Hourly electricity providers after transmission lines for Coastal BLEL, in 2030 (node 1).

installation is relatively lower and the system is balanced with a shift towards more PV with lower FLh and consequently more HVAC.

The role of battery storage in providing total BLEL demand or total electricity demand for *Onsite* BLH$_2$ is illustrated in Fig. 21. Battery does not contribute to supplying electricity to electrolysers for *Onsite* BLH$_2$ in 2030, while in 2050 it has a minor role in the cost-optimised configuration. On the other hand, battery has a significant role in providing BLEL. Battery supplies about 35%–55% of BLEL demand in regions with more than 80% PV installed capacity (Fig. 19). This observation that solar PV can be effectively balanced with battery storage is also found in Breyer et al. (2017). As the costs of PV and battery storage decline, global shares of PV and battery storage increase from 2030 to 2050.

As illustrated in Fig. 22, gas turbines supply a relatively smaller share of *Onsite* BLEL in comparison to batteries in PV-dominated regions, but have a bigger share in wind-dominated regions. In most of Europe, Central Northern America and Southern Argentina, hydrogen-fuelled gas turbines supply 15%–25% of *Onsite* BLEL in 2030. The role of gas turbines increases to about 35% at latitudes above 80°N with less favourable wind conditions and strong solar seasonality. The role of gas turbines in providing BLEL decreases in 2050 as hybrid PV-battery systems become a cheaper solution in more regions.

As illustrated in Fig. 23, the overall efficiency of *Onsite* BLEL in 2030 ranges from 61% to 90%, with the upper range representing regions with the lowest losses, which consist of curtailed electricity and losses in the battery and PtH$_2$tP cycles, including the electricity requirement of compressors. In the *Coastal Scenario*, the losses are higher due to additional transmission lines and conditional AC/DC converter losses and the overall efficiency ranges from 55% to 88%. The efficiency decline is close to zero at coastal nodes and gradually increases to 14–17% in the farthest nodes from open sea in north-west China. Despite higher curtailment levels in 2050, the overall efficiencies are relatively higher, as more regions are PV-dominated, coupled with significantly higher shares of cheaper and more efficient batteries, which in turn reduces the share of the less energetically efficient PtH$_2$tP system. The efficiency improvement of HVDC transmission lines and converters also contributes to the overall efficiency increase of remote areas in the *Coastal Scenario* in 2050.

While the electrolyser efficiency is 82.3%, the overall efficiency of power to *Onsite*BLH$_2$ in 2030 is about 69.7–81.9% worldwide, as shown in Fig. 24. The additional losses consist of zero to 12% electricity curtailment and less than 1% electricity consumption by hydrogen compressors, depending on the FLh of the electrolysers and the respective hydrogen storage demand. In the *Coastal Scenario*, the overall losses increase by up to 21% in remote areas,
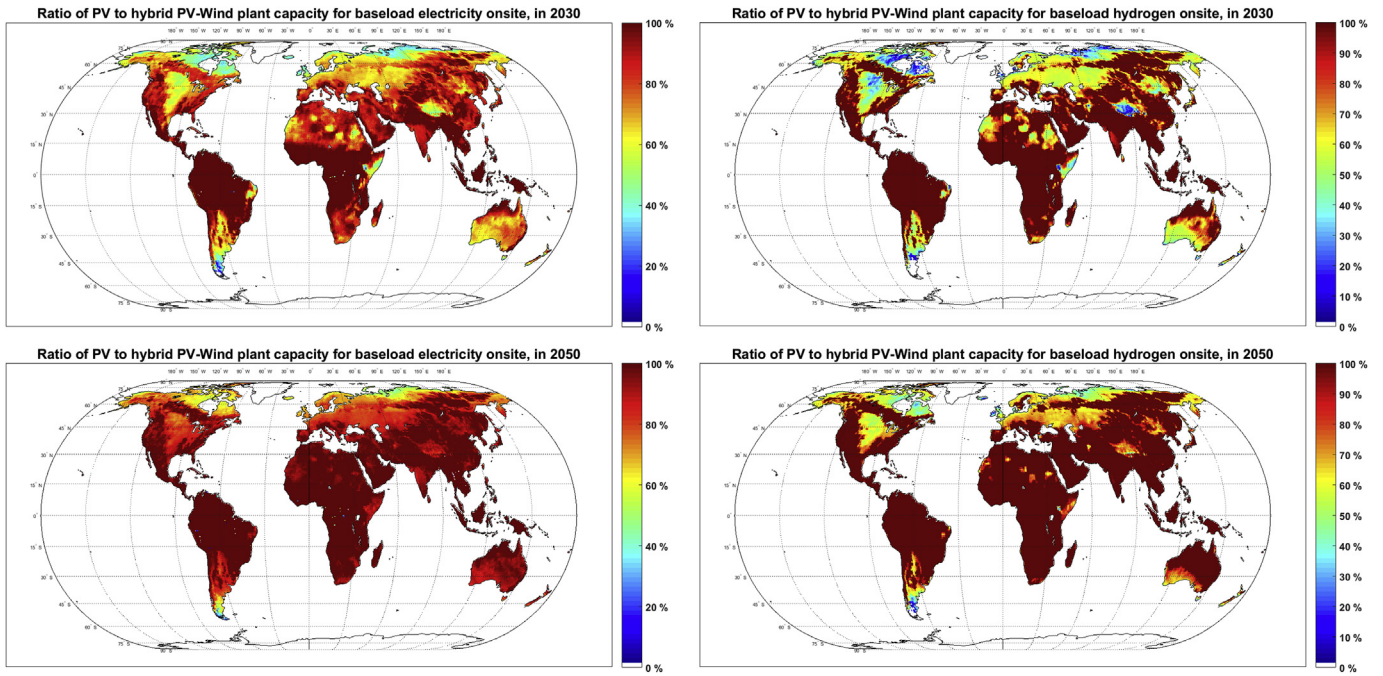
Fig. 19. Ratio of PV to hybrid PV-wind installed capacity for *Onsite* BLEL (left) and BLH$_2$ (right) for 2030 (top) and 2050 (bottom).
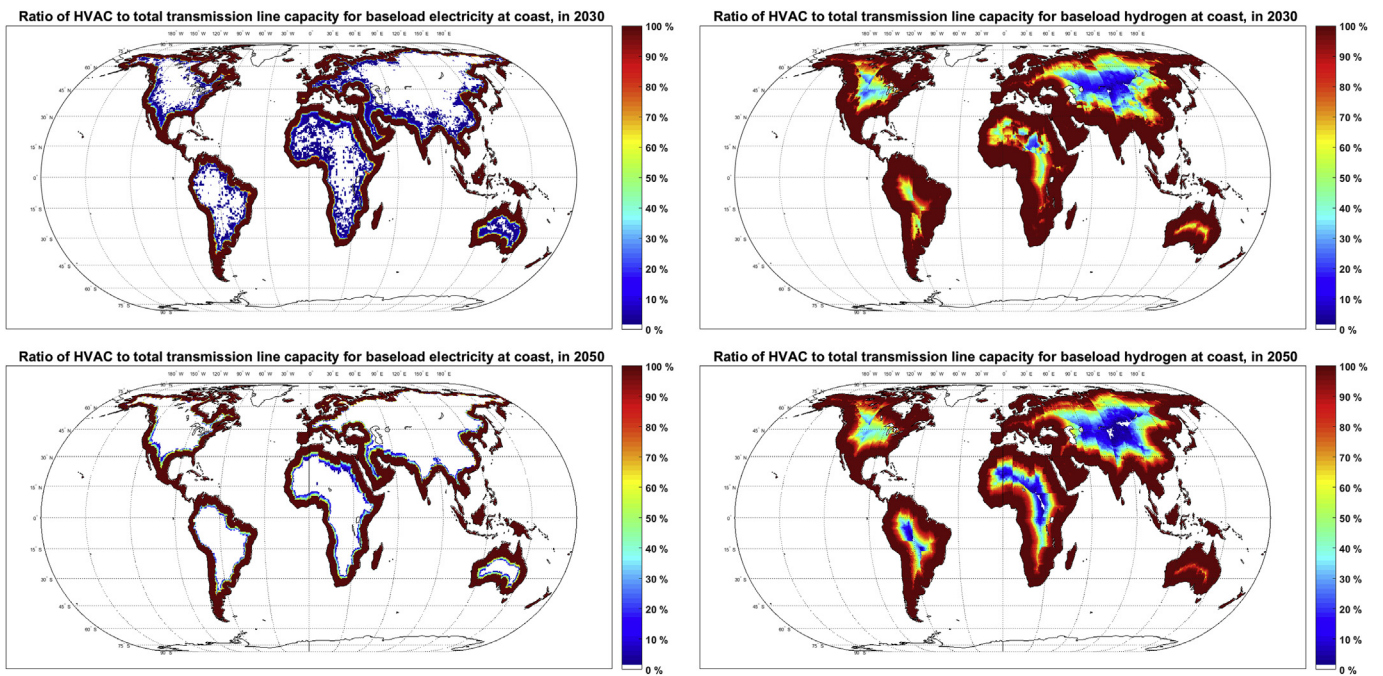

Fig. 20. Ratio of HVAC to HVAC and HVDC capacity for *Coastal* BLEL (left) and BLH$_2$ (right) for 2030 (top) and 2050 (bottom).

leading to an overall efficiency of about 51.9–81.5%, due to efficiency losses in long-distance transmission lines, higher curtailment levels and losses in the battery storage cycle in remote areas for increasing transmission lines utilisation rates as a part of the cost-optimised solution. The distance impact on overall efficiency would make regions close to the coastal line a better option for harvesting solar and wind energy for export purposes. In 2050, the overall efficiency of the *Onsite Scenario* in most regions slightly

decreases by about 0–9% in comparison to 2030, as electricity becomes cheaper and, along with losses in the battery cycle, higher levels of curtailment become a more competitive balancing solution. This finding has also been observed in other energy system analyses as documented by Solomon et al. (2019). On the other hand, the overall efficiency of the *Coastal Scenario* in 2050 increases as batteries, PtH$_2$tP systems and transmission lines become more efficient.
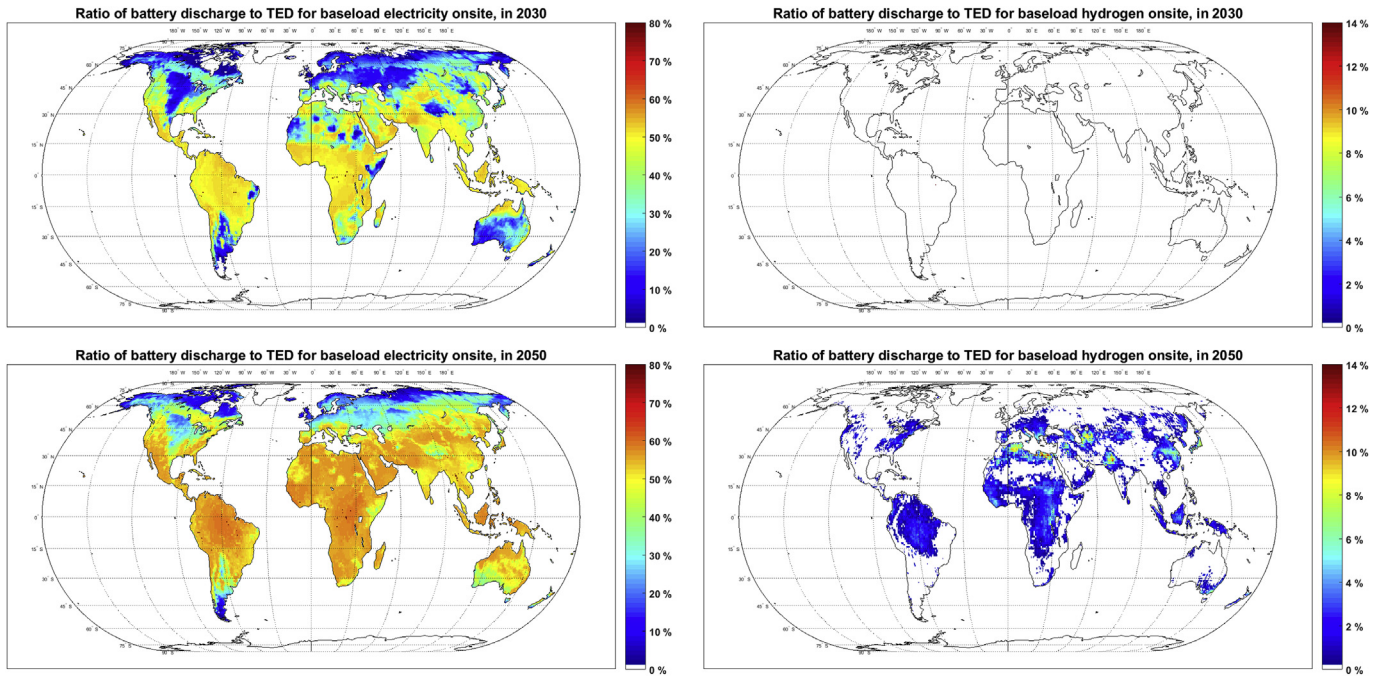
Fig. 21. Ratio of battery discharge to total electricity demand (TED) for BLEL (left) and BLH$_2$ (right) *Onsite* for 2030 (top) and 2050 (bottom).
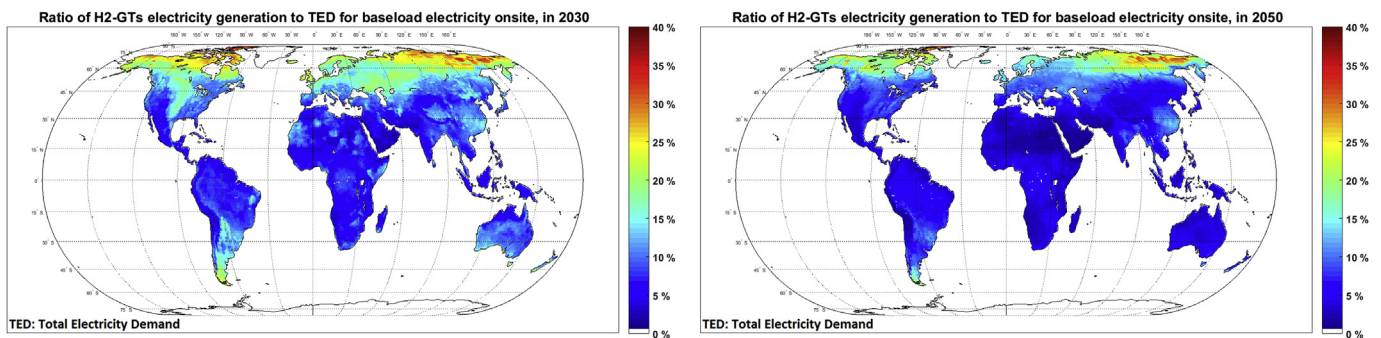

Fig. 22. Ratio of hydrogen-fuelled gas turbines (CCGT and OCGT) generation to total electricity demand (TED) for BLEL *Onsite* in 2030 (left) and 2050 (right).

3.5. BLEL and BLH$_2$ annual capacity and generation potential

As discussed in the Methods section, a maximum 10% of land at each node can be allocated to solar PV or wind power plants for BLEL or BLH$_2$ generation. The nodal hosting capacity of PV and wind power plants and their respective annual generation based on 2005 weather data are shown in Fig. 25. With the average land use assumptions in this study, the hosting capacity of a given area of solar PV is about 9 times higher than that of wind power plants; however, the ratio of actual output capacity would be lower, due to lower output power rates set by inverter capacity for PV systems. At about 18.6 and 2.1 GW, nodes at the equator have the highest hosting capacities for PV systems and wind power plants, while the hosting capacities halve towards the polar nodes as the nodal area decreases (Fig. 3). Based on PV and wind FLh in 2005 (Fig. 4), such capacities of wind power plants, fixed tilted PV and single-axis tracking PV can annually generate up to 11, 38 and 44 TWh of electricity, respectively.

Not all the potential hosting capacities may be utilised in the cost-optimised configuration. For example, in a PV-dominated cost-optimised system, the 10% land allocated to wind is not used.

Accordingly, the optimal nodal capacity potentials of BLEL and BLH$_2$ in 2030 are shown in Fig. 26. At more than 4 GW$_p$ and 3.5 GW$_{H2}$, the Atacama Desert, Northern Australia, Southern Saudi Arabia and most of Africa have the highest nodal optimised capacities for BLEL and BLH$_2$ generation, respectively. In the *Coastal Scenario*, the generation capacities of BLEL and BLH$_2$ decrease, due to efficiency losses discussed in Section 3.4.

Based on the global baseload capacities in Fig. 26, the global generation potential of cost-optimised BLEL or BLH$_2$, with 10−20% area coverage, is close to 1 million TWh$_{el}$ or 1 million TWh$_{H2,HHV}$ in 2030. To put things in perspective, the global total primary energy demand in 2017 was about 162,500 TWh$_{th}$ (IEA, 2018), which may not exceed 400,000 TWh$_{el}$ in a mainly electrified world by the end of the 21st century (Breyer et al., 2017). The total generation potential also increases over time as the role of solar PV strengthens, which can generate more electricity per area everywhere. It is not taken into account that solar PV systems and wind power plants can be built at the same site as an on-site integrated hybrid PV-wind power plant (Ludwig et al., 2019). Such integrated plants further increase the energy yield per area and may have lower total system costs due to better shares of land costs and in particular grid
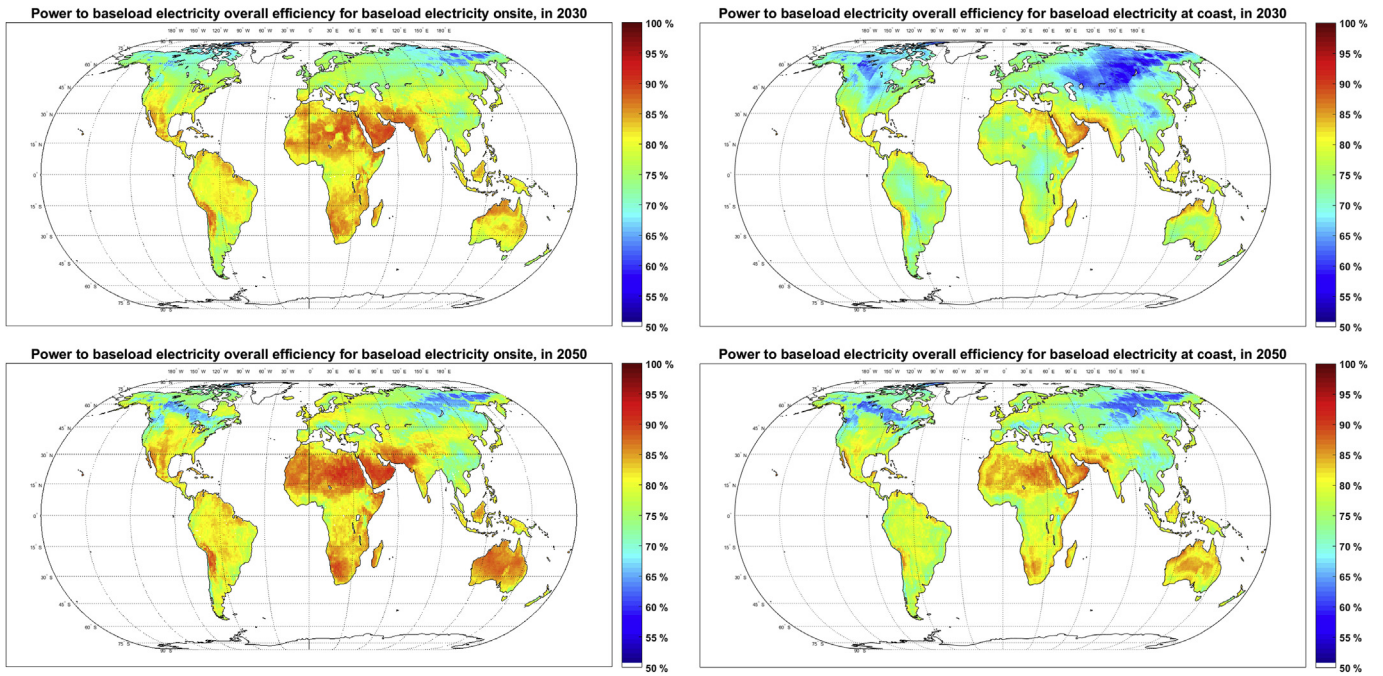
Fig. 23. Power to BLEL overall efficiency *Onsite* (left) and *Coastal* (right) for 2030 (top) and 2050 (bottom).
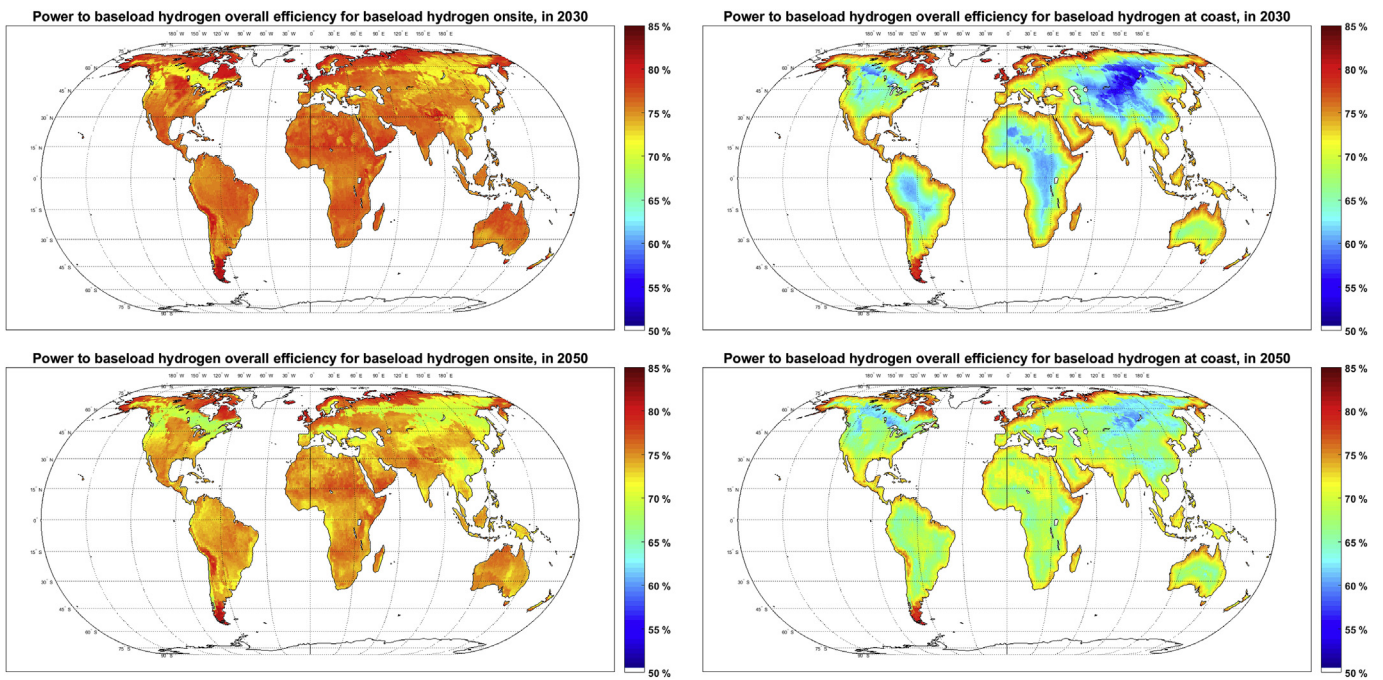
Fig. 24. Power to BLH$_2$ overall efficiency *Onsite* (left) and *Coastal* (right) for 2030 (top) and 2050 (bottom).

connection and power transmission costs. However, only capacities at affordable cost levels are desired. In Fig. 27, the global generation potential of BLEL and BLH$_2$ in all years and scenarios are sorted based on the generation costs.

In addition to demand by chemical and metal refining industries, BLH$_2$ would be mostly needed for synthetic fuels and chemicals, which can be produced at the best sites of the world and the final product can be shipped to target markets at relatively lower costs. Thus, both *Onsite* and *Coastal* hydrogen production

could have a major role. Considering the total primary energy demand, the first 200,000 TWh$_{th,HHV}$ BLH$_2$ would be more than enough to meet any kind of baseload hydrogen demand, leaving space for any uncertainty with land availability or other types of power demand. For up to 200,000 TWh$_{th,HHV}$ BLH$_2$ at the coast (for production and export of synthetic fuels and chemicals), the generation costs could decline from 39 to 88 €/MWh$_{H2,HHV}$ in 2020 to about 31−61, 28−51 and 26−44 €/MWh$_{H2,HHV}$ in 2030, 2040 and 2050 respectively, based on the higher heating value of hydrogen.
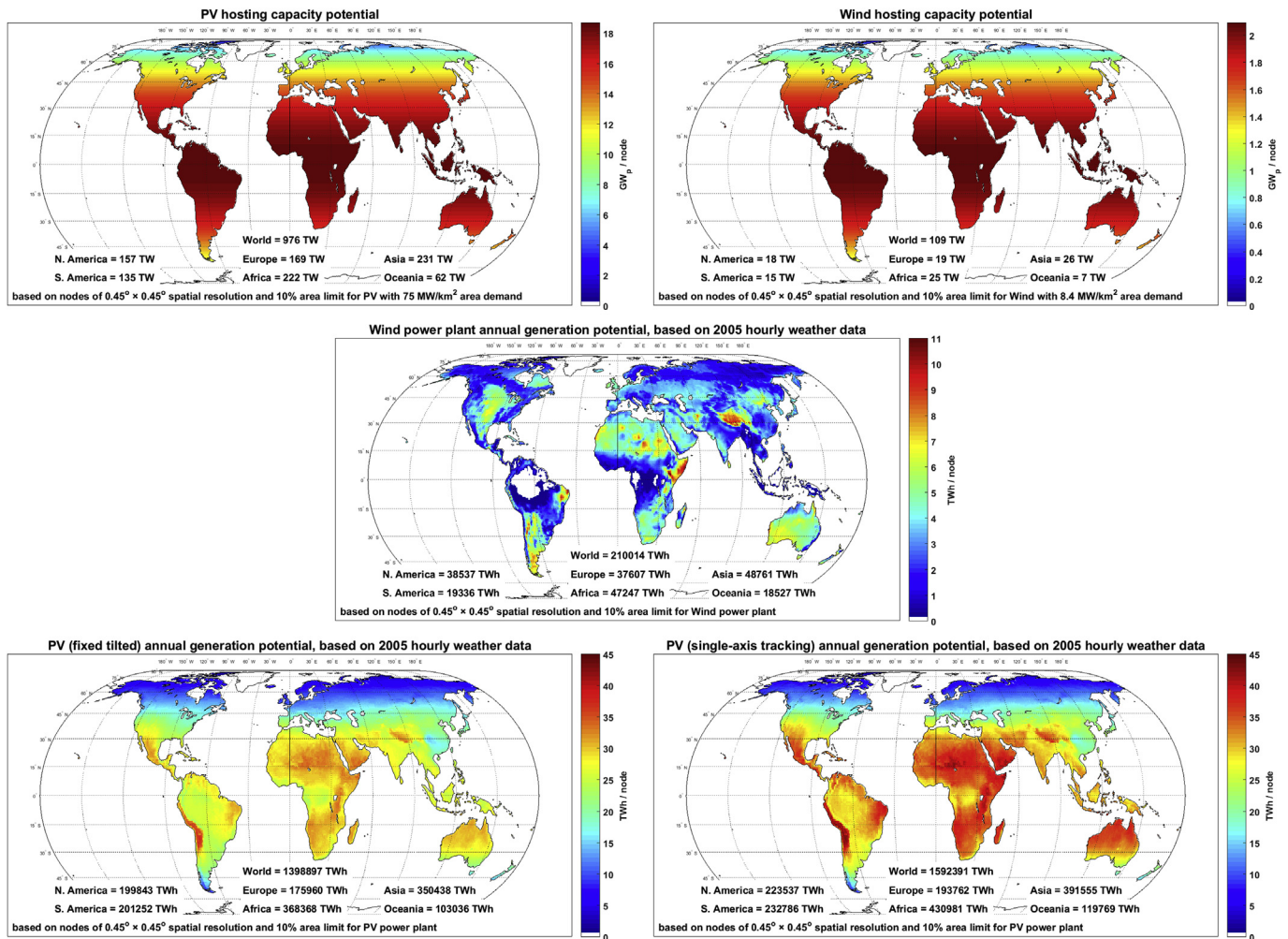
Fig. 25. Hosting capacity potential for PV systems (top left) and wind power plants (top right), annual generation potential for wind power plants (centre), fixed tilted PV (bottom left) and single-axis tracking PV (bottom right) based on 10% land use limit for PV and wind power plants for 2005 weather data. The specific values are based on nodes of the size of $0.45° \times 0.45°$ spatial resolution.

For *Onsite*BLH$_2$, the world is divided into 9 major regions (Fig. S19) and the generation costs of the first 5000 TWh$_{th,HHV}$ *Onsite*BLH$_2$ in each region for 2030 and 2050 is shown in Table 2. Although Europe has some potential for cheap *Onsite* hydrogen production, the cost increases relatively rapidly for higher production levels, which could make it a region with a land limitation for low-cost *Onsite* BLH$_2$ generation. Thus, Europe is more likely to have *Onsite* hydrogen generation for hydrogen needed by chemical and steel industries, while synthetic fuels are imported from regions that can provide cheap hydrogen at scale. The full production cost range for 2020 to 2050 is available in Figure S21.

The transmission of BLEL over long distances or overseas would be relatively expensive (Breyer et al., 2019b). Thus, regional availability of BLEL is of higher importance. As pointed out in the introduction, BLEL would be mainly part of a variable electricity supply and met by a mix of resources and technologies. However, to address requirements for a more theoretical consideration, the generation costs of the first 5000 TWh *Onsite* BLEL for each major region for 2030 and 2050 are shown in Table 2 and the full range for all years is illustrated in Figure S20. The generation of BLEL in 2020, with no seasonal electricity balancing option in the model, starts at costs between 104 and 140 €/MWh in all 9 major regions but cannot scale in Europe and Eurasia, while in the MENA region and Sub-Saharan Africa it remains below 120 €/MWh for the first

5000 TWh *Onsite* BLEL generation. *Onsite* BLEL costs drop significantly in 2030 with some generation capacity below 60 €/MWh in all major regions, with further cost decline to about 31−47 in 2050, with Sub-Saharan Africa, South America, the MENA region and Northeast Asia as the lower limit and Europe and Eurasia as the upper limit. As such, the costs of RE-BLEL would become competitive with the costs of available conventional baseload generators (Ram et al., 2018) in most parts of the world by 2030.

4. Discussion

For the sake of model consistency, GTs were also included as an electricity supplier to electrolysers for BLH$_2$ production in the Matlab models, as for BLEL models. However, as was expected, GTs did not become part of the cost-optimised solution and were thus not shown and discussed in the methods and results sections. Not being a part of a cost-optimised solution is not because of financial or efficiency assumptions, but the lack of logic behind the power-to-H$_2$-to-power-to-H$_2$ loop. Under no conditions such a loop would be meaningful.

4.1. Cost difference of the Onsite and Coastal Scenarios

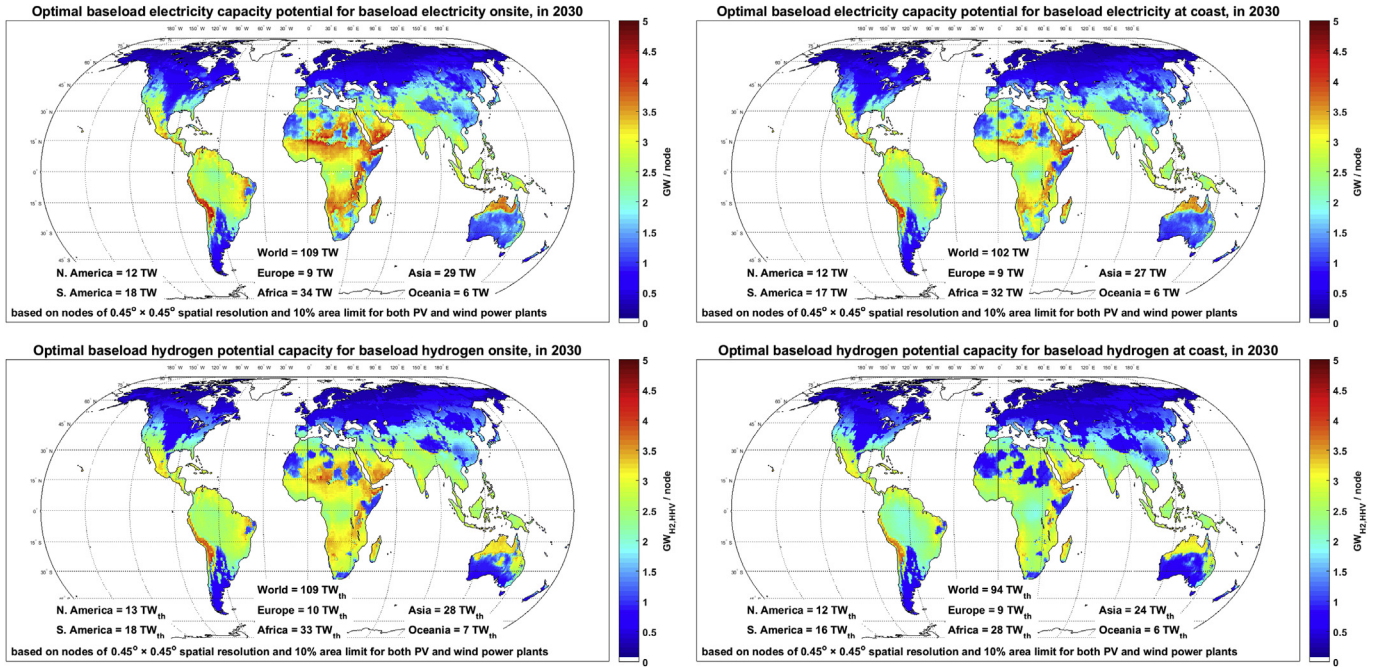The cost difference of the *Coastal* and *Onsite* BLEL or BLH$_2$

Fig. 26. BLEL (top) and BLH$_2$ (bottom) optimal capacity potential for *Onsite* (left) and *Coastal* (right) scenarios in 2030 with 10% land use limit for PV and wind power plants. The specific values are based on nodes of the size of 0.45° × 0.45° spatial resolution.
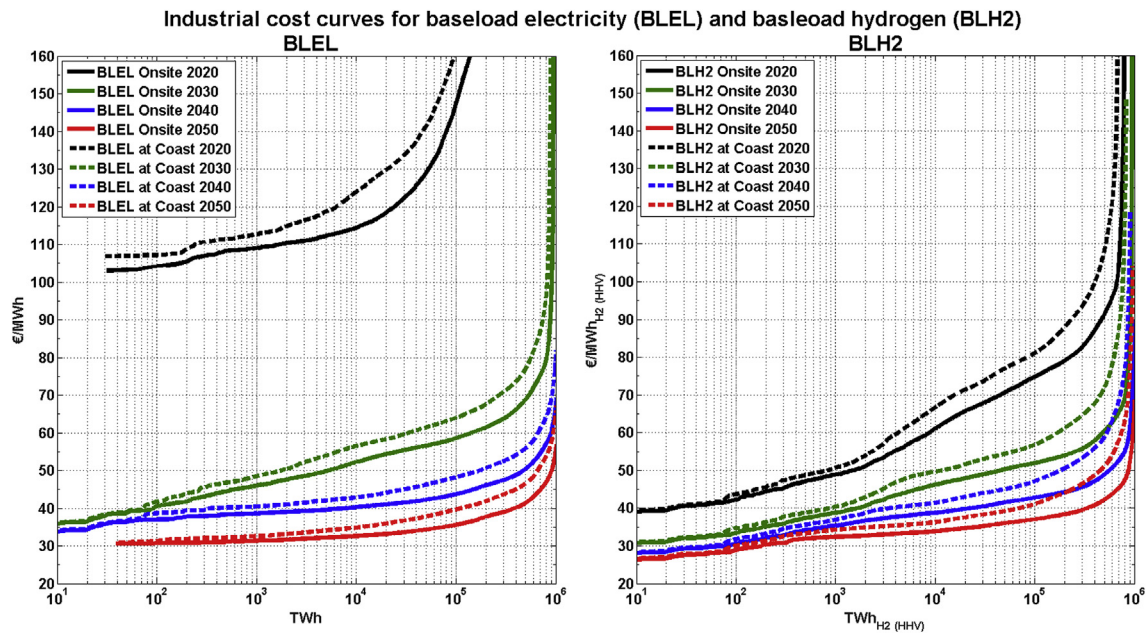

Fig. 27. Industrial cost curves for BLEL (left) and BLH$_2$ (right), based on cost-optimised hybrid PV-wind power plants for the period 2020 to 2050.

scenarios is zero at coastlines and grows by increasing distance from the coast, as shown in Fig. 28. The additional cost of transmission lines for BLH$_2$ is almost double the cost for BLEL per unit of energy, because BLEL is already balanced before the transmission line, while for BLH$_2$ such a condition is not needed in the *Onsite Scenario*, and higher capacities of transmission lines or balancing technologies are thus needed. In 2050, the cost differences at 1000 km decrease to about 5−10 €/MWh (about 17% in reference to *Onsite*) and 10−17 €/MWh$_{th}$ (about 32% in reference to *Onsite*) for BLEL and BLH$_2$, respectively. Such low electricity transmission costs

in the future open doors for harvesting low-cost electricity in remote areas, eliminating concern about land use in urban areas.

4.2. Sensitivity analyses

The input financial and efficiency assumptions in any global study include some degree of uncertainty regarding long-term projections and regional operational condition. For example, although PV solar power plant equipment could be delivered all around the world at almost even cost, the construction costs

Table 2
BLEL and BLH$_2$ generation cost range for the first 5000 TWh BLEL or 5000 TWh$_{H2,HHV}$ BLH$_2$ generation in 9 major regions, based on cost-optimised hybrid PV-wind power plants.

Region	BLEL (€/MWh)		BLH$_2$ (€/MWh$_{H2,HHV}$)	
	2030	2050	2030	2050
Europe	48−70	41−47	39−62	34−45
Eurasia	55−72	38−47	44−62	38−46
MENA	50−56	31−33	47−50	33−35
Sub-Saharan Africa	41−53	31−33	36−48	31−35
SAARC	52−64	36−38	43−56	36−40
Northeast Asia	43−56	32−35	37−51	32−36
Southeast Asia	48−57	35−38	42−51	35−37
North America	50−60	36−38	43−52	35−38
South America	40−54	31−33	33−46	28−34

depend on terrain conditions. Alternatively, harsh desert weather conditions might decrease the technical lifetime of PV modules. Such regional impacts are not considered in the presented global simulations.

On the other hand, WACC is maybe the most decisive non-technical factor in the final cost of each project and it could be time and location dependent. All the simulations in this study have been based on 7% WACC as an average global number. However, as development and stability indices enhance in developing countries in the long term, their required WACC for investments and consequently global average WACC could be lowered. In addition, as RE-based technologies mature and scale up, the investment risks decline, which would consequently lower the WACC. Therefore, a lower global average WACC could be expected in the long term. As a generic sensitivity analysis, the global costs of *Onsite* BLEL and BLH$_2$ in 2050 based on 5% WACC are illustrated in Fig. 29, which show about 15% reduction in final product costs in comparison to 7% WACC all around the globe.

In the short term, regional investment stability would affect the associated WACC. Latest findings for the case of solar PV and onshore wind power plant investments in Germany for 2017 indicate WACC as low as 2.5% (solar PV) and 2.75% (wind power plants) based on current exceptional macroeconomic conditions and the risk profile of RE investments in Germany (Egli et al., 2018). On the other hand, investors expect higher WACC in less stable and financially developed regions. As a case study, levelised cost of BLEL and BLH$_2$ in Germany and Kenya have been compared for an equal WACC of 7% and unequal WACC ranges of 3−5% and 10−15% in Germany and Kenya, respectively. Considering the lifetime of units, this could result in about 15−28% BLH$_2$ cost reduction in Germany and 24−68% BLH$_2$ cost increase in Kenya, in reference to the basic WACC of 7%.

The results illustrated in Fig. 30 show that under equal WACC conditions of 7%, BLEL and BLH$_2$ could be generated at 10 to 30 €/MWh lower cost in Kenya for 2030 conditions. However, factoring in the local WACC conditions, the production costs in Germany would become competitive with those in Kenya. For a WACC of 5% in Germany and 10% in Kenya, the production costs of the first 500 TWh$_{el}$ or TWh$_{H2,HHV}$ at best sites is comparable, while any lower WACC in Germany or higher WACC in Kenya would lead to cheaper BLEL or BLH$_2$ production in Germany. As an example, for a more realistic WACC of 3% in Germany and a theoretical WACC of 15% in Kenya, the production cost of BLEL and BLH$_2$ at the best sites in Germany would be about 25−30 €/MWh lower than Kenya. Increasing regional jobs, supply security and avoiding transportation costs of energy carriers could be other incentives for Germany favouring local or regional supply of secondary energy. However, the land use constraints in meeting local demand and the acceptance of scaled solar PV and wind power plants by German society needs to be evaluated.

According to the cost distribution illustrated in Fig. 15, PV and wind power plants have the biggest cost share in *Onsite* BLEL and BLH$_2$ systems, while battery and electrolyser units are the other capex intensive units for BLEL and BLH$_2$, respectively. Battery degradation is about 20% during a lifetime of 20 years (Samsung SDI, 2018), which could add 10% to the investment cost. However, the unexpectedly sharp decline in battery cost in today's market is beyond the cost decline assumptions in this study, which may make
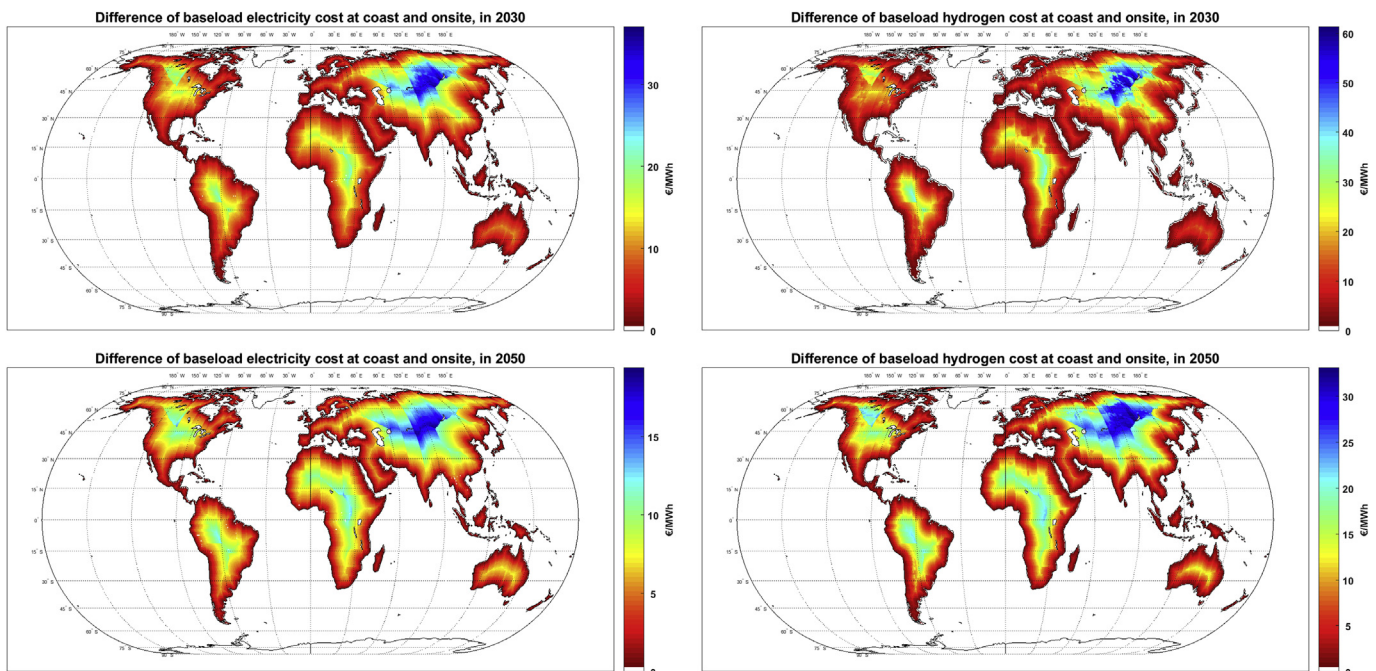

Fig. 28. Cost difference of the *Coastal* and *Onsite Scenarios* for BLEL (left) and BLH$_2$ (right) for 2030 (top) and 2050 (bottom).
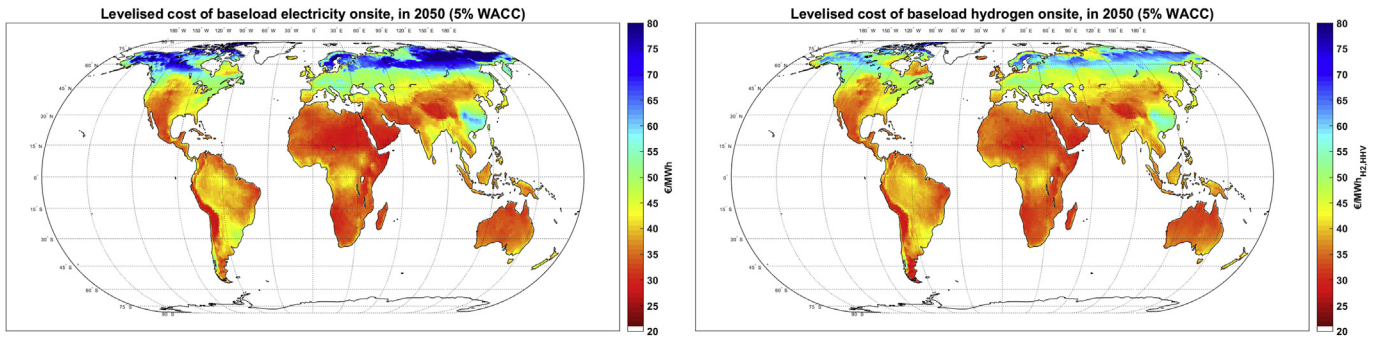
Fig. 29. Levelised cost of baseload electricity (left) and baseload hydrogen (right) *Onsite* with 5% WACC in 2050.
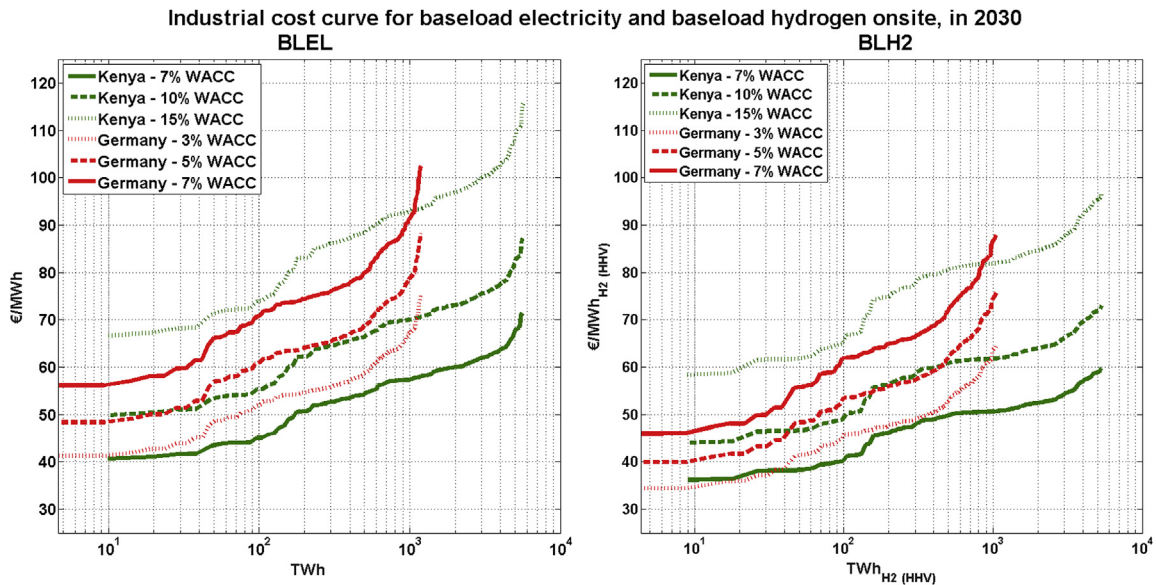

Fig. 30. Levelised cost of baseload electricity (left) and baseload hydrogen (right) for Germany and Kenya for 2030 with globally equal and localised WACC.

the current assumptions conservative. In addition, H_2-based gas turbines play a significant role in BLEL production, while achieving capital expenditures at the level of conventional NG-based gas turbines, which faces some uncertainties. Thus, a generic sensitivity analysis of capex of PV, wind, battery and gas turbines for *Onsite* BLEL and capex of electrolysers for *Onsite* BLH_2 in 2030 has been performed. The impact of 10% change in the capex of the above-mentioned units with fixed absolute opex has been illustrated in Fig. 31.

A 10% change in the capex of PV and wind results in 0−4% and 0−6% change in the overall costs of BLEL. A 10% change in battery costs shows the same impact as PV on the costs of BLEL in 2030 and in the same regions, since they are mainly coupled. Results show that a 10% increase in capital expenditures of gas turbines could lead to just zero to 1.5% increase in total costs of BLEL in 2030, with the maximum in wind dominated regions (Fig. 31). In all cases, the impact is minimised by cost-optimising through rebalancing the system with a different combination of technologies according to the new cost assumptions.

As shown in Fig. 32, a 10% capex change of the water electrolyser has less than 2% impact on the overall costs of BLH_2, observed mainly in wind dominated regions. During the finalisation of this study, new information was found about large-scale hydrogen compressors with considerably lower capital expenditures and relatively higher electricity demand of 100 €/kW$_{H2}$ and 0.045 kWh/

kW$_{H2}$ (Grond et al., 2013). Applying the new specifications for hydrogen compressors results in up to 11% reduction of BLH_2 in 2030 in PV-based regions which need high daily compression of hydrogen. In addition, the Nel Group expects large-scale electrolysers with a capex less than 500 USD/kW (about 500 €/kW$_{H2,HHV}$) (NEL, 2017). This is about 27% lower in cost than the applied electrolyser capex for 2020 in this study, which together with the lower compressor cost can reduce hydrogen production cost in 2020 by about 15−20%. The lower capex for 2020 would also have a respective impact on the applied capex in later years according to the learning rate.

4.3. Close to baseload electricity

As discussed in section 3.2, with no long-term storage option in 2020, maintaining baseload electricity would require considerably higher installed capacities of battery storage and solar PV or wind power plants to decrease storage demand, which significantly increases the cost of BLEL in many regions. Such conditions could also affect regions with relatively good solar and wind power potential, even if they face power deficits for only several days in a row. In such conditions, rethinking demand management could be as crucial as supply management. Such impact could be lower for 2030 and beyond as the respective model includes PtH_2tP systems as seasonal electricity storage. Fig. 33 illustrates the cost of variable
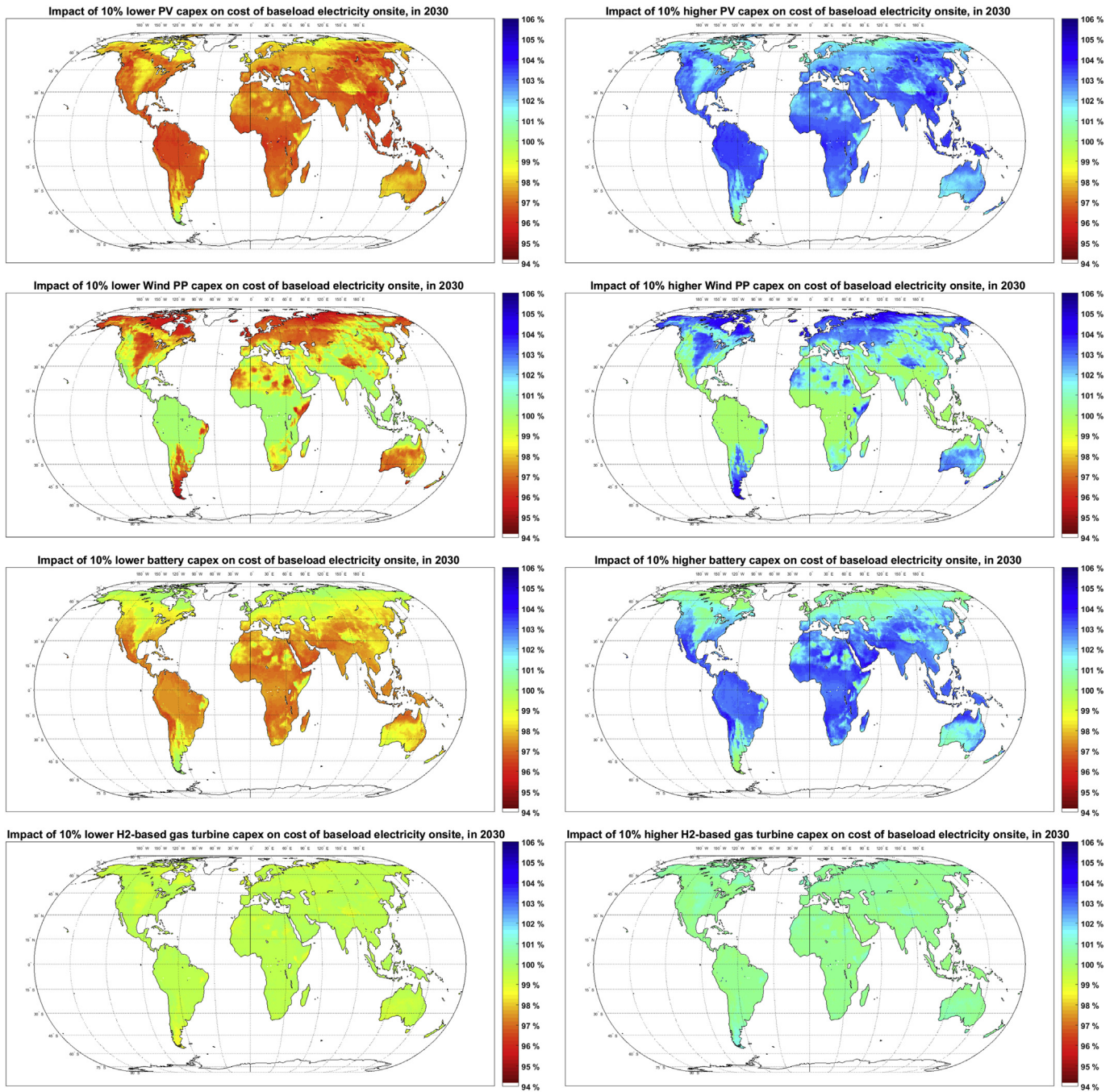
Fig. 31. Impact of PV capex (top), Wind capex (upper centre), battery capex (lower centre) and gas turbines capex (bottom) on levelised cost of BLEL *Onsite* in 2030.

load electricity (VLEL) with 8000 FLh in 2020, 2030, 2040 and 2050. For 2020, the results show about 20−80% electricity cost reduction around the world. In the Atacama Desert and the Arabian Peninsula, impact is the lowest at about 20−30%, due to stable solar conditions throughout the year. Regardless of excellent wind FLh of about 5000−6200 h in Patagonia, the adjusted requirement to 8000 FLh reduces the cost for the delivered electricity by about 60−80%. For 2030 and beyond, the impact of decrease in FLh on the cost of electricity is significantly lower as the model is supplied by the PtH$_2$tP system as the seasonal electricity balancing option. In 2030, the cost reduction is about 10−15% in most regions, while it is up to 25% in low-cost nodes with high shares of wind. This decrease in FLh would also lower the role of H$_2$-CCGT as a seasonal electricity

supplier and H$_2$-OCGT would be fully eliminated. In 2050, more regions would gain a 20−25% cost reduction and elimination of GTs in a variable load electricity system with 8000 FLh.

Although industry prefers baseload operation to maximise production, lowering FLh could provide a financial incentive for those capable of operating under slightly variable load in exchange for lower electricity cost. For example, a study by Breyer et al. (2019) shows that the cost-optimised solution for capex intensive CO$_2$ direct air capture systems powered by hybrid PV-wind-battery systems in the Maghreb region would have FLh of 8000−8400 h. Another example is the near to baseload operation conditions for seawater reverse osmosis desalination plants on the Arabian Peninsula at about 8400−8700 FLh (Caldera and Breyer, 2018),
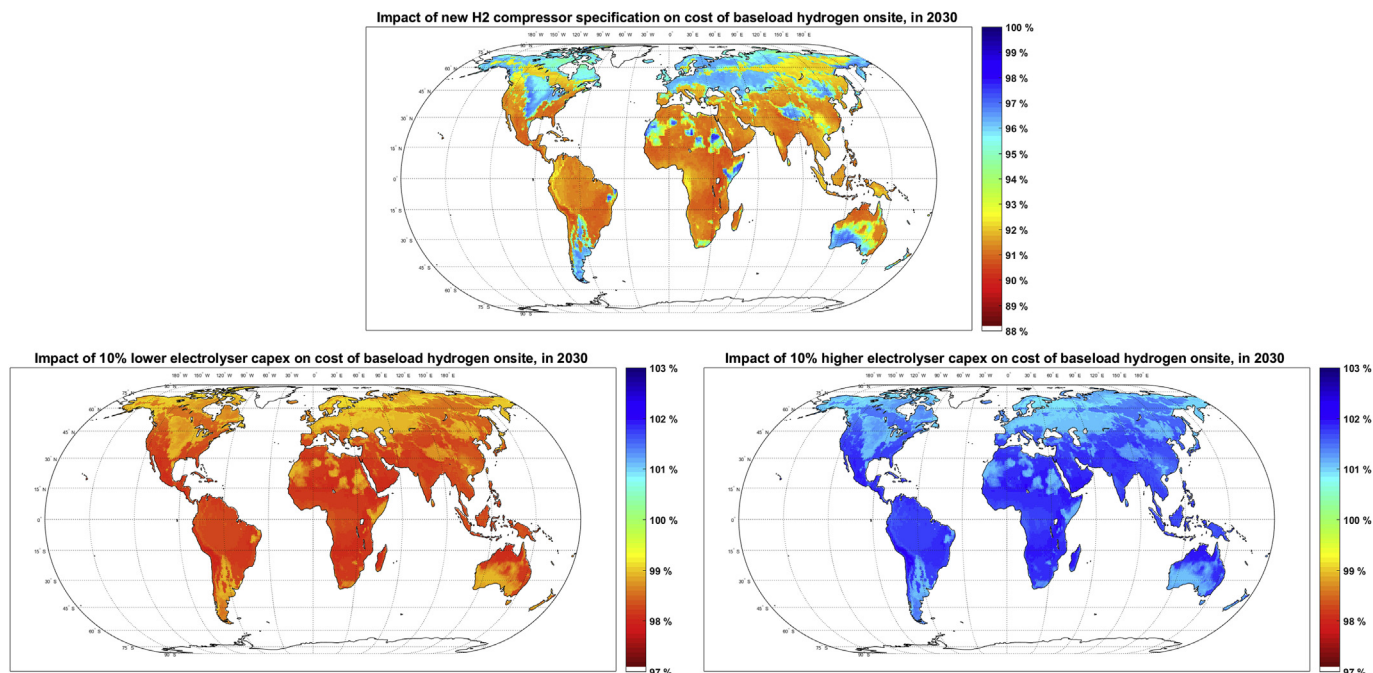
Fig. 32. Impact of electrolyser capex on levelised cost of BLH$_2$ *Onsite* in 2030.

which can be technically operated in a more flexible mode but require high FLh for cost-optimised operation.

Close to baseload supply, with 8000 FLh, could be the toughest imaginable condition that solar and wind power generation could face in a grid connection, as in most parts of the world there could be some regional dispatchable renewable resource such as hydro reservoirs or bioenergy to fill the gap to BLEL if needed. According to Sepulveda et al. (2018), in a low-cost scenario for all grid suppliers in northern and southern US, solar PV power would be dominant and futuristic low-cost and flexible nuclear power plants would not be part of the cost-optimised mix of deployable technologies. This cost-optimised mix of technologies emphasises the difference between reliable balancing solutions and the burden of expensive baseload or even flexible nuclear. In addition, the low-cost PV assumption of 670 USD/kW$_{AC}$ for the year 2047 by Sepulveda et al. (2018) is higher than current capex levels of 575−650 USD/kW$_{AC}$ (USD/€ exchange rate of 1.2) in India (Fortum, 2018a, 2018b). This capex collation shows the competitiveness of today's solar PV with promised low-cost nuclear, while the solar PV cost decline is ongoing at a high rate (ITRPV, 2019; ETIP PV, 2019). It is worth mentioning that the capex in literature is mainly based on PV panels' nominal capacity (per kW$_p$) and the conversion factor is about 1.35 of kWp/kW$_{AC}$. As such, the capex for the Indian project is 356 €/kW$_p$ in 2019, which is below the capex assumptions of fixed tilted PV for 2030 in our study.

4.4. Fossil vs. RE-based BLH$_2$

The cost of hydrogen generated via steam methane reforming (SMR) depends on the cost of fossil NG, which has generally been a function of crude oil prices. The ratio of NG to OECD crude oil prices is illustrated in Fig. 34. The long-term average price ratio of NG to OECD crude oil prices in Germany, the UK, the Netherlands, USA and Canada based on the available data in Fig. 34 are 77%, 62%, 58%, 60% and 45%, respectively, averaged for the last 34, 22, 13, 29 and 28 years, respectively, BP (2018). The average price of LNG delivered to Japan has been 102% of crude oil prices in the past 34 years BP

(2018). The price ratio of regasified LNG in Japan would be 8%−3% higher for a crude oil price range of 30−150 USD/bbl, based on regasification costs reported by Fasihi et al. (2017).

The SMR-based hydrogen production costs in Fig. 35 are based on given crude oil and respective NG prices and SMR plant specifications in Table 3.

The cost comparison of RE-BLH$_2$ and SMR-H$_2$ was performed for four scenarios with 40%, 60%, 80% and 100% NG to crude oil price ratios representing the different regional costs of NG. The impact of respective CO$_2$ emission costs of 28, 61, 75 and 150 €/t$_{CO2}$ in 2020, 2030, 2040 and 2050 (BNEF, 2015; Bogdanov et al., 2019) on SMR-H$_2$ were also studied. RE-BLH$_2$ costs are based on the maximum generation costs of 20,000 TWh$_{H2,HHV}$ per year from best sites in the world, which are about 66, 48, 40 and 35 €/MWh$_{H2,HHV}$ in 2020, 2030, 2040 and 2050, respectively. In 2020, at 66 €/MWh$_{H2,HHV}$, RE-BLH$_2$ could be cost competitive with SMR-H$_2$ at a crude oil price of about 100 USD/bbl and 100% NG to crude oil price ratio or at a crude oil price of about 135 USD/bbl and a NG to crude oil price ratio of 80%. With current trends, crude oil prices over 100 USD/bbl seem unlikely in 2020 and an NG to crude oil price ratio of about 100% could only be expected in Japan. With a general WACC of 7%, the RE-BLH$_2$ generation costs at best sites in Japan in 2020 would be about 80 €/MWh$_{H2,HHV}$, relatively higher than the chosen RE-BLH$_2$ cost index for 2020, however, the generation cost would be comparable for a localised WACC of 5%. In addition, lower generation costs than 66 €/MWh$_{H2,HHV}$ are achievable at so-called sweet spots (Fig. 12). For example, the generation costs could be as low as 42−46 €/MWh$_{H2,HHV}$ in Patagonia or 50−56 €/MWh$_{H2,HHV}$ in Iceland, UK and Ireland or 57−61 €/MWh$_{H2,HHV}$ in Denmark, Quebec (Canada), and South Dakota (US). Some of above-mentioned regions and countries could adopt a WACC of 5% or less, which would decrease the generation cost by more than 15%. As such, RE-BLH$_2$ generation costs at best sites (geographically and economically) could be as low as 40−45 €/MWh$_{H2,HHV}$, equal to the reference generation cost in 2040 for mass production. At such sites, RE-BLH$_2$ can become cost competitive with SMR-H$_2$ in 2020 for crude oil prices of about 67−83 USD/bbl (lower range for applied CO$_2$
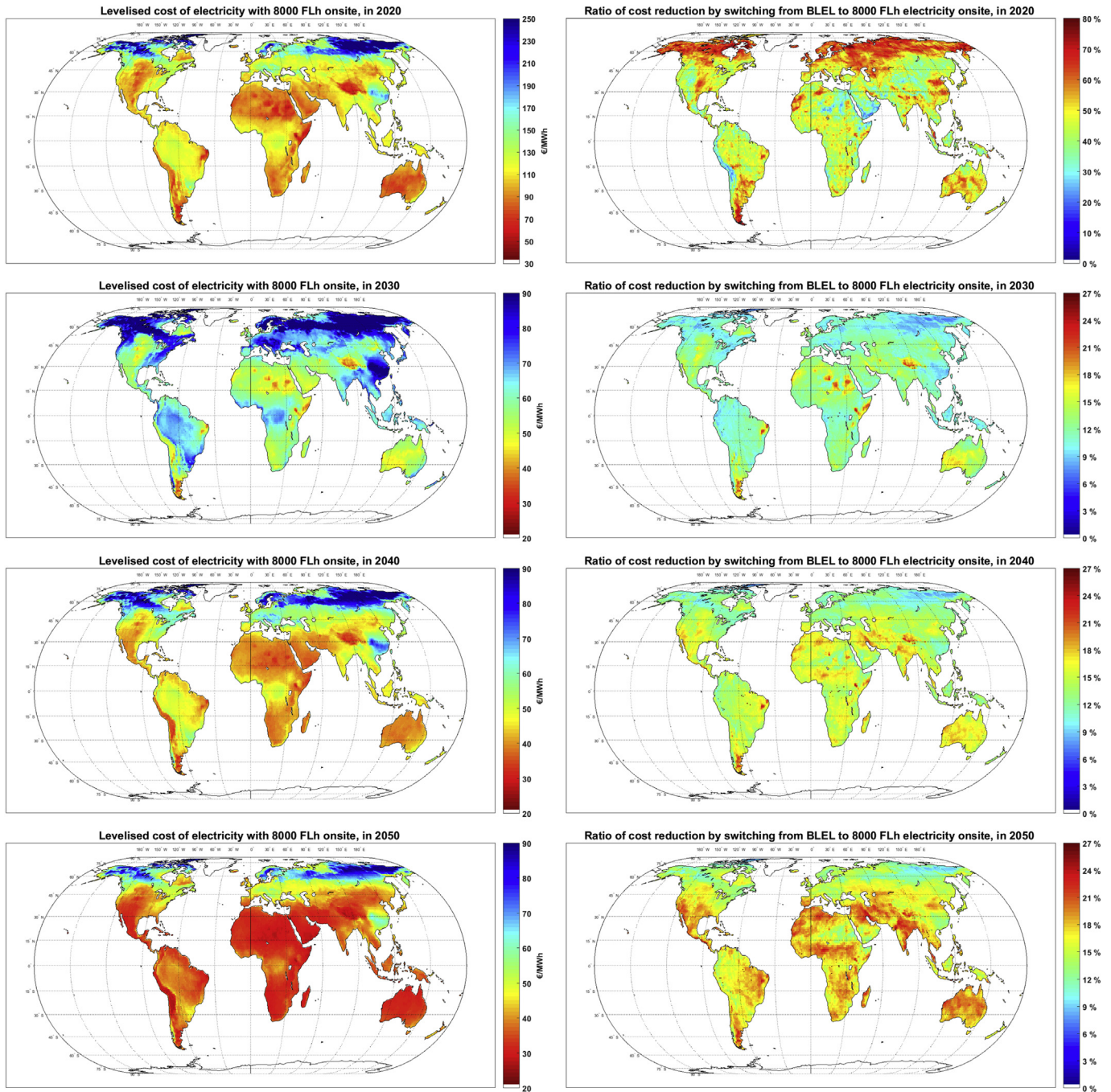
Fig. 33. Levelised cost of variable load electricity for 8000 FLh in the years 2020−2050 for the *Onsite Scenario* conditions in absolute LCOE (left) and relative cost reduction in reference to the baseload case (right).

emission cost) and a NG to crude oil price ratio of 80%. The annual generation capacity of such sites in 2020 would be limited, but nevertheless in the scale of TWh$_{th}$ (Fig. 27) and enough for the entry level expansion of such a route to the global market. In 2040, the RE-BLH$_2$ generation cost of 40 €/MWh$_{H2,HHV}$ under the reference scenario coupled with 75 €/t$_{CO2}$ emissions costs can reach fuel parity at 54 or 40 USD/bbl for a NG to crude oil price ratio of 60% or 80%, respectively, which indicates the importance of such emission controlling policies at national and international levels. In the reference scenario, achieving such generation cost levels in Europe would still be limited to some coastal regions. However, a more realistic WACC of 3−5% for European countries would make such

cost levels achievable in most of southern and western Europe. The other option would be to import RE-H$_2$ from best spots in the world, namely Patagonia and the Atacama desert, at costs of about 32−34 €/MWh$_{H2,HHV}$. However, the additional costs of shipping hydrogen to Europe has to be considered, as discussed by Heuser et al. (2019).

In 2050, a CO$_2$ emissions cost of 150 €/t$_{CO2}$ would make RE-BLH$_2$ at best sites cost competitive with SMR-H$_2$ at any crude oil price and NG to crude oil price ratio level. However, since SMR provides a pure source of CO$_2$, the CO$_2$ capture process is relatively affordable and it might be possible to capture, transport and safely store that fossil CO$_2$ for lower cost. If so, this would be the logical choice for
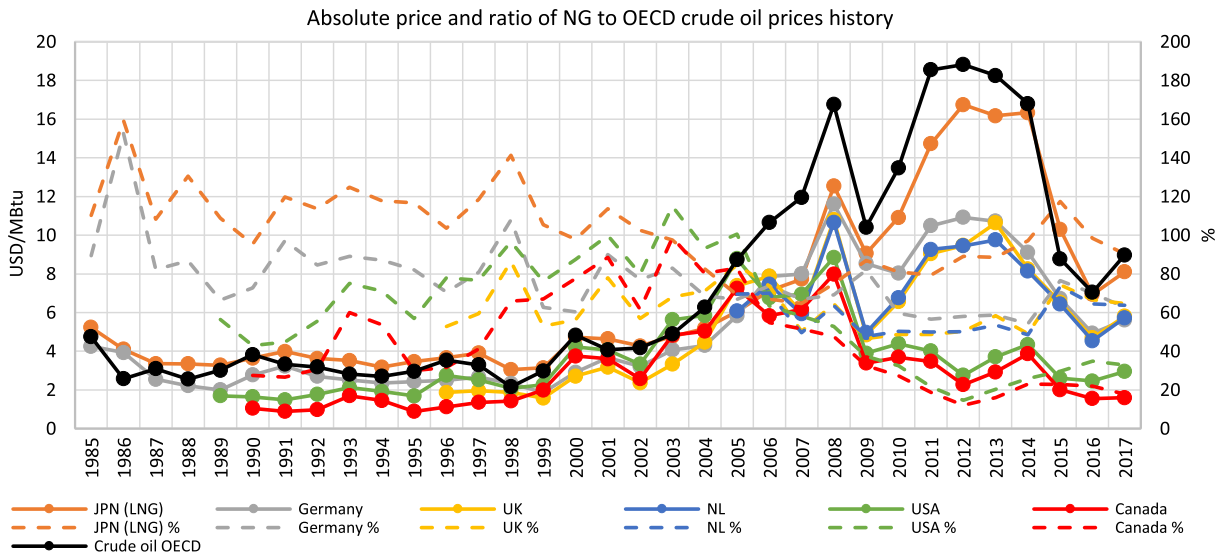
Absolute price and ratio of NG to OECD crude oil prices history

Fig. 34. Absolute price and ratio of NG to OECD crude oil prices history. Data taken from BP (2018).

the SMR industry to avoid higher CO_2 emission penalties. Nevertheless, gaseous CO_2 storage may not be a safe storage option and a scalable CO_2 storage in the form of a chemically inert solid material with a high combustion point is needed like, for instance, the enhanced weathering carbon mineralisation route practiced in Iceland (CarbFix, 2018). CO_2 injection and monitoring cost for carbon mineralisation in the Iceland project is in the range of 2−4.2 €/$t_{CO2,injected}$ (Gunnarsson et al., 2018) and has a carbon mineralisation efficiency of about 72 ± 5% (Pogge von Strandmann et al., 2019). CarbFix (2018) considers offshore carbon mineralisation in submarine basalts as a natural and environmentally safe solution with significant storage capacity. To offset the CO_2 loss of the storage chain, an equivalent amount should be captured and stored through direct carbon capture and storage (DACCS) or respective carbon emission costs should be applied to the losses of the chain. In the case of no point source carbon capture, a full carbon emission penalty or an equivalent amount of DACCS are the options. Fig. 36 shows a cost comparison of carbon capture, transport and storage with these methods within a probable cost range for each technology.

As illustrated in Fig. 36, SMR-based PSCC costs 5−40 €/t_{CO2} in 2020 (Fasihi et al., 2019). Since the CO_2 source is relatively pure, only a slight cost decline of the upper limit to 34 €/t_{CO2} is considered. On the other hand, DAC cost ranges from 133 to 235 €/t_{CO2} in 2020, with the lower limit representing sites with excellent solar conditions and free access to waste heat for CO_2 regeneration (Fasihi et al., 2019) The higher limit represents the same configuration but in a region without access to free waste heat and a single-axis tracking system with 1500 FLh. Even though DAC scaling is expected to decrease the CO_2 capture cost significantly by mid-century, the least cost DAC scenario would not become cheaper than high cost carbon capture from a SMR plant. Considering CO_2 transportation cost of 2−25 €/t_{CO2} (Fasihi et al., 2019), a CO_2 storage cost of 3−15 €/$t_{CO2,injected}$, and a CO_2 mineralisation rate of 72%, CO_2 direct air carbon capture, transport and storage (DACCTS) in 2020 would be in the range of 192−383 €/$t_{CO2,mineralised}$, which could decrease to 52−136 and 40−114 €/$t_{CO2,mineralised}$ by 2050 and 2100, respectively. Point source carbon capture, transport and storage (PSCCTS) should pay the penalty for carbon losses in the respective year. Consequently, PSCCTS in 2020 would be in a range of 18−88

€/$t_{CO2,mineralised}$, which, unlike DACCST, increases to 52−117 €/$t_{CO2,mineralised}$ by 2050 and stabilises at this cost level until the end of century. As a result, paying for CO_2 emission cost seems the cheapest option for the SMR industry in 2020, even though it does not offset the actual emissions. As the CO_2 emissions cost increases, the CO_2 emissions penalty and PSCCTS would rise to the same cost level in 2030−2040. However, PSCCTS should be prioritised in this situation, because if the emissions are released to the atmosphere, offsetting the emissions through DACCTS would cost more. In 2050 and beyond, PSCCTS and DACCTS could be at the same cost range of 50−120 €/$t_{CO2,mineralised}$, i.e. significantly lower than the selected CO_2 emission cost of 150 €/t_{CO2}. Thus, self-neutralisation of CO_2 emissions would be the least-cost option for the SMR industry. In addition, the cost of methane leakage through NG production, transportation and the SMR process should be taken into account, as it has a much higher global warming impact than NG. On the other hand, for an average 75 €/t CO_2 neutralisation cost in 2050, RE-H_2 could be cost competitive with fossil SMR-H_2 at 55, 37, 30 USD/bbl or below 30 USD/bbl for a NG to crude oil price ratio of 40%, 60%, 80% and 100%, respectively. Thus, SMR-based H_2 would not be cost competitive with RE-based H_2 in 2050 in the first place and the RE-based H_2 route could eliminate the need for CO_2 capture and storage for hydrogen generation. Substitution of SMR-based H_2 with RE-based H_2 is particularly important, as the global CO_2 storage capacity would be better used for neutralisation of unavoidable CO_2 emissions, such as those from the cement industry.

In 2017, NG and crude oil consumption in Europe were about 5600 and 9000 TWh$_{th}$, respectively (BP, 2018), which was partly used to meet Europe's 280 TWh$_{th}$ hydrogen demand (EC, 2015). Europe's capacity for producing globally cost-competitive synthetic H_2-based fuels and chemicals would be limited. However, as hydrogen has higher transportation costs than other gaseous or liquid energy carriers, meeting direct hydrogen demand by onsite production could be expected as the first choice at best sites in Europe, while more dense gaseous or liquid synthetic fuels could be generated at lower cost sites and then shipped to Europe for the lowest transportation costs. On the other hand, the oil and NG production costs of major suppliers are below 20 USD/bbl (IEA, 2008; IEA, 2009; Knoema, 2019), which can compete with all the above scenarios except the case with 150 €/t_{CO2} emissions costs.
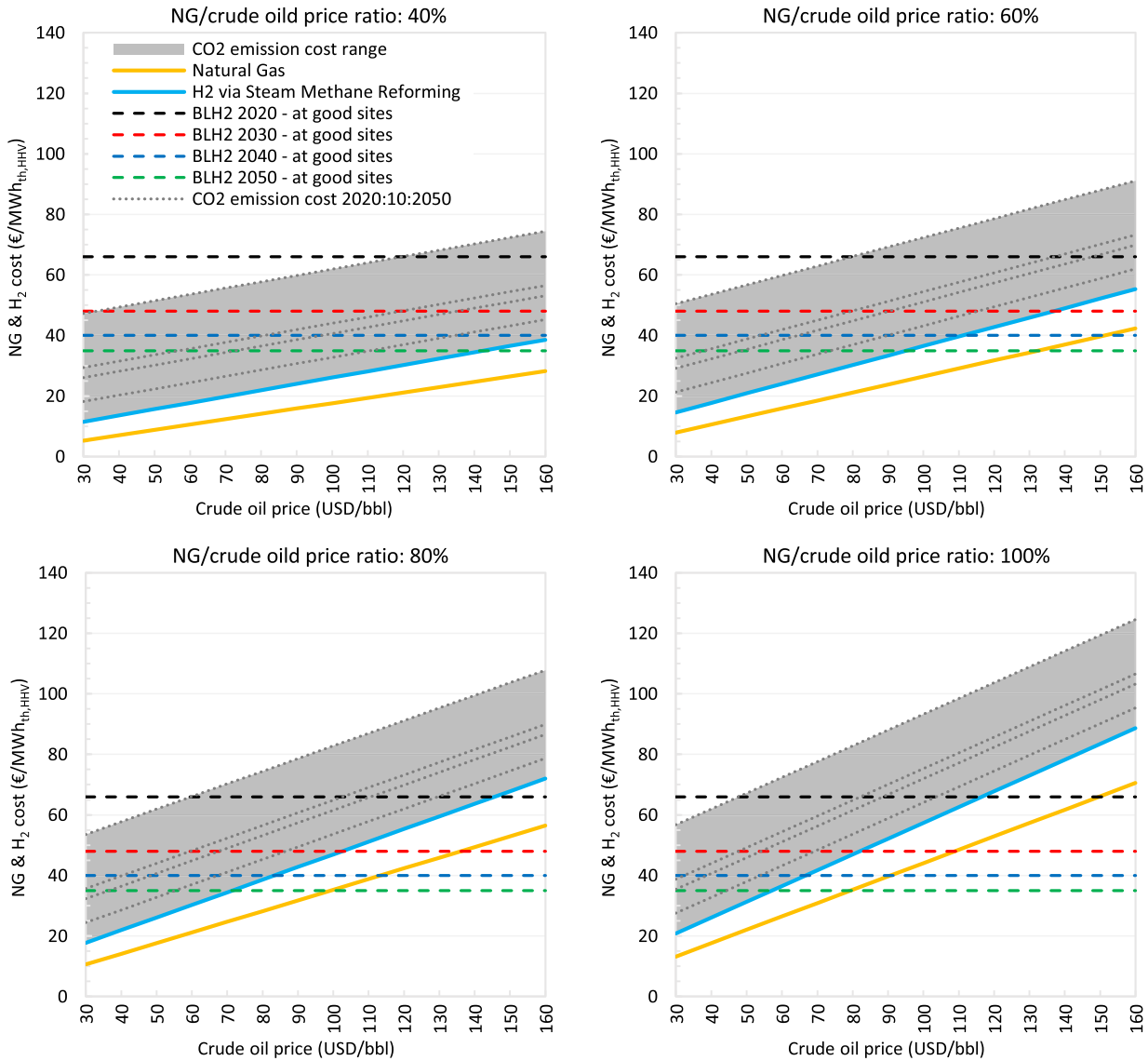
Fig. 35. RE-based BLH$_2$ vs SMR-based H$_2$ for different natural gas prices.

Table 3
Steam methane reforming plant specifications.

	unit	2020−2050	reference
capex	€/kW$_{H2,HHV}$	320	IEA (2015)
opex fix	% of capex p.a.	5	
eff. (HHV)	%	84.5	IEA (2015)
lifetime	year	30	IEA (2015)
availability	h	8000	

4.5. By-products

The electrolyser in a 1 GW$_{H2,HHV}$ BLH$_2$ system would generate about 1.75 million tonne of oxygen and 870 GWh$_{th}$ of low-grade heat (below 100 °C), annually, which could partly provide additional value through regional circular economy opportunities, such as district heating or as main energy input to low temperature direct air capture systems (Fasihi et al., 2019). According to Fasihi et al. (2019), supply of low temperature heat by heat pump and heat storage could cost about 36 €/MWh$_{th}$ by 2020 in the Maghreb region with some of the best solar and wind resources in the world.
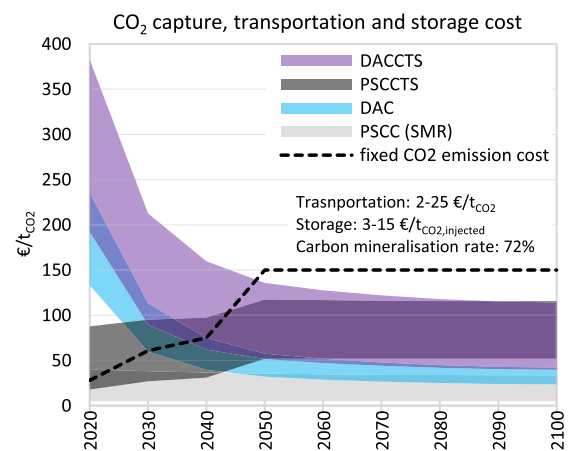

Fig. 36. Estimated cost range of PSCCTS and DACCTS from 2020 to 2100.

Accordingly, a low temperature heat price of $20-40$ €/MWh$_{th}$ can generate $2-4$ € extra revenue per MWh$_{H2,HHV}$ and decrease the hydrogen generation cost by about $5-10\%$. While this might not be a significant advantage for hydrogen generation, in an integrated system with direct air capture, free low-grade heat can reduce the cost of CO_2 direct air capture by about 40% Fasihi et al. (2019).

The growing oxygen market reached 438 Mt$_{O2}$ in 2006, with the steel industry accounting for about 48% as the main consumers. However, oxygen demand from the steel industry would end as a result of substitution of coal with hydrogen (Fischedick et al., 2014). The chemical industry is the sector with the second-largest oxygen demand, about 19% of total demand (Gasworld, 2007). This demand level is equal to about 83 Mt$_{O2}$, which can be generated as a by-product of 47.4 GW$_{H2,HHV}$ BLH$_2$ or 415 TWh$_{H2,HHV}$ H$_2$. Thus, the oxygen market is relatively small, especially since bulk demand is usually generated onsite to avoid liquefaction and transportation costs. However, in the case of an occasional match, profit from oxygen sales could be significant. Water electrolysis would generate 0.2 t$_{O2}$/MWh$_{H2,HHV}$, which with a $45-100$ €/t$_{O2}$ price (Intratec, 2018) can generate $9-20$ € profit per MWh$_{H2,HHV}$, thus increasing the competitiveness of green hydrogen with steam methane reforming.

5. Conclusion

In this study, *Onsite* and *Coastal Scenario* supply of BLEL and BLH$_2$ via cost-optimised hybrid PV-wind-battery power plants are modelled. The simulations are based on hourly weather data in a $0.45° \times 0.45°$ spatial resolution and results are reported for cost and efficiency assumptions in the years 2020, 2030, 2040 and 2050.

The hourly analyses show that hybrid PV-wind power plants can provide BLEL at affordable costs in most regions around the world, if coupled with proper daily and long-term balancing technologies. The scenario analysis results show that, for 7% WACC, 5000 TWh$_{el}$ BLEL can be generated at the best sites of each of the 9 major regions studied at a cost range of $104-220$, $39-72$, $37-57$ and $30-48$ €/MWh in 2020, 2030, 2040 and 2050, respectively. The lower limit of the given range represents the generation cost in Sub-Saharan Africa, South America, the MENA region and Northeast Asia and the upper limit represents mainly Europe and Eurasia. Thus, even though BLEL may remain a theoretical demand, the proposed system is capable of providing BLEL at the same cost level as conventional sources by 2030 in most parts of the world.

The absence of seasonal electricity balancing technology in the 2020 model results in over-dimensioning of the system and high curtailment levels and it has the highest impact on BLEL production costs. In addition, an electricity exchange between battery storage and PtH$_2$tP system is observed, which minimises the required capacities and costs. Higher round trip efficiency and lower cost of power-to-hydrogen-to-power in comparison to power-to-SNG-to-power could make H$_2$-based gas turbines a complementary daily balancing solution to battery power even in PV-dominated systems in 2030. However, their role could diminish by 2050 due to the expected sharp decline of battery cost.

Although BLEL may mainly remain a theoretical demand, off-grid close-to-BLEL demand is expected to rise for applications such as water desalination and CO_2 direct air capture. The results of this work show that in the absence of seasonal storage technology in the 2020 model, variable load electricity at 8000 FLh could be $20-80\%$ cheaper than BLEL in 2020, with the highest range in wind-dominated areas. For the years 2030 and beyond, with a seasonal electricity storage option, the cost reduction is in the range of $10-25\%$.

On the other hand, providing BLH$_2$ appears to be technically less challenging, as well-known widespread hydrogen cavern storage is the only required balancing solution. Batteries are not expected to have a significant role in providing electricity for *Onsite* hydrogen production by water electrolysers. However, as PV-based systems become more favourable, the role and cost share of hydrogen compressors increases. Results show that for 7% WACC at best sites with maximum 200,000 TWh$_{H2,HHV}$ annual cumulative generation potential, BLH$_2$ can be generated at $39-88$, $31-61$, $28-51$ and $26-44$ €/MWh$_{H2,HHV}$ in 2020, 2030, 2040 and 2050, respectively.

BLH$_2$ is needed for production of synthetic fuels and chemicals and as a substitute for SMR in meeting direct hydrogen demand from the chemical industry. The cost competitiveness of RE-BLH$_2$ with SMR depends on the green hydrogen generation cost, the price of crude oil and local NG/crude oil price ratios and applied CO_2 emission cost rates. The results of this study show that cost competitiveness of RE-BLH$_2$ with SMR is achievable in 2020 for a limited capacity in the best matching scenario (high RE potential, low WACC, high crude oil and NG/crude oil prices), while the cost decline of renewables and expected increase in CO_2 emission costs beyond 2020 could make RE-H$_2$ cost competitive with SMR on all continents.

Although solar and wind potential power is not the best in central Europe, supportive policies by government, higher CO_2 emission cost, lower investment risks and WACC can improve local generation competitiveness. In Northeast Asia (namely Japan and South Korea), land limitations could be a problem for scaling local production. Nevertheless, export of renewable energy from the best sites in the world to such regions via high voltage transmission lines or in the form of transportable energy carriers such as synthetic fuels remains an option. The results presented in this work show that the financially justified electricity transmission distance from best sites in the world is limited to about 1000 km.

Future research is needed on the possibility and cost of hydrogen transportation via pipelines and in liquefied form around the globe in comparison to electricity transmission lines. In addition, high spatial resolution maps of geologically suitable sites for hydrogen caverns are needed for a more accurate simulation. Moreover, more research is needed on the best mix of hydrogen compressor, buffer and cavern.

The results of this study suggest that clean and cost-competitive sources of reliable electricity and hydrogen can substitute conventional fossil and nuclear sources, which will contribute to cleaner production of electricity or hydrogen consuming products. In addition, defossilisation of hydrogen generation could be the first step in substitution of other conventional fuels with RE-based synthetic fuels.

Appendix A. Supplementary data

Supplementary data to this article can be found online at https://doi.org/10.1016/j.jclepro.2019.118466.

References

Afanasyeva, S., Bogdanov, D., Breyer, C., 2018. Relevance of PV with single-axis tracking for energy scenarios. Sol. Energy 173, 173−191.

Aghahosseini, A., Bogdanov, D., Barbosa, L.S.N.S., Breyer, C., 2019. Analysing the feasibility of powering the Americas with renewable energy and inter-regional grid interconnections by 2030. Renew. Sustain. Energy Rev. 105, 187−205.

Agora Energiewende, 2014. Stromspeicher in der Energiewende; Agora energiewende: Berlin, Germany. September. Available online: https://goo.gl/RHMAvk. (Accessed 4 January 2019).

Anicic, B., Trop, P., Goricanec, D., 2014. Comparison between two methods of methanol production from carbon dioxide. Energy 77, 279–289.

BNEF, 2015. New Energy Outlook 2015 - Long-Term Projections of the Global Energy Sector, vol. 2015. Bloomberg New Energy Finance, London.

Bogdanov, D., Breyer, C., 2016. North-East Asian Super Grid for 100% renewable energy supply: optimal mix of energy technologies for electricity, gas and heat supply options. Energy Convers. Manag. 112, 176–190.

Bogdanov, D., Farfan, J., Sadovskaia, K., Aghahosseini, A., Child, M., Gulagi, A., Oyewo, A.S., Barbosa, L.S.N.S., Breyer, C., 2019. Radical transformation pathway towards sustainable electricity via evolutionary steps. Nat. Commun. 10, 1077.

Bolinger, M., Seel, J., Hamachi LaCommare, K., 2017. Utility-Scale Solar 2016 -An EmpiricalAnalysis of Project Cost, Performance and Pricing Trends in the United States. Lawrence Berkeley National Laboratory, Berkeley, September. Available at: https://utilityscalesolar.lbl.gov. (Accessed 24 December 2018).

BP, 2018. BP Statistical Review of World Energy 2018, 67th Edition. BP, London. Available online: https://on.bp.com/2DcWxJf. (Accessed 24 January 2019).

Breyer, C., Heinonen, S., Ruotsalainen, J., 2017. New Consciousness: a societal and energetic vision for rebalancing humankind within the limits of planet Earth. Technol. Forecast. Soc. Chang. 114, 7–15.

Breyer, C., Bogdanov, D., Aghahosseini, A., Gulagi, A., Child, M., Oyewo, A., Farfan, J., Sadovskaia, K., Vainikka, P., 2018. Solar photovoltaics demand for the global energy transition in the power sector. Prog. Photovolt. Res. Appl. 26, 505–523.

Breyer, C., Fasihi, M., Aghahosseini, A., 2019a. Carbon dioxide direct air capture for effective climate change mitigation: a new type of energy system sector coupling. Mitig. Adapt. Strategies Glob. Change 1–23. https://doi.org/10.1007/s11027-019-9847-y (in press).

Breyer, C., Bogdanov, D., Aghahosseini, A., Gulagi, A., Fasihi, M., 2019b. On the Techno-Economic Benefits of a Global Energy Interconnection (submitted).

Brown, T.W., Bischof-Niemz, T., Blok, K., Breyer, C., Lund, H., Mathiesen, B.V., 2018. Response to 'Burden of proof: a comprehensive review of the feasibility of 100% renewable-electricity systems'. Renew. Sustain. Energy Rev. 92, 834–847.

Caldera, U., Breyer, C., 2017. Learning curve for seawater reverse osmosis desalination plants: capital cost trend of the past, present and future. Water Resour. Res. 53, 10523–10538.

Caldera, U., Breyer, C., 2018. The role that battery and water storage play in Saudi Arabia's transition to an integrated 100% renewable energy power system. Journal on Energy Storage 17, 299–310.

Caldera, U., Bogdanov, D., Breyer, C., 2016. Local cost of seawater RO desalination based on solar PV and wind energy: a global estimate. Desalination 385, 207–216.

CarbFix, 2018. The CarbFix project fact sheet. Orkuveita Reykjavíkur, Reykjavík. Available online: https://bit.ly/2YqqugF. (Accessed 14 May 2019).

Child, M., Koskinen, O., Linnanen, L., Breyer, C., 2018. Sustainability guardrails for energy scenarios of the global energy transition. Renew. Sustain. Energy Rev. 91, 321–334.

Chisalita, D.-A., Cormos, C.-C., 2019. Techno-economic assessment of hydrogen production processes based on various natural gas chemical looping systems with carbon capture. Energy 181, 331–344.

Dana, A.G., Elishav, O., Bardow, A., Shter, G.E., Grader, G.S., 2016. Nitrogen-based fuels: a power-to-fuel-to-power analysis. Angew. Chem. Int. Ed. 55, 8798–8805.

DECHEMA, 2017. Low Carbon Energy and Feedstock for the European Chemical Industry. DECHEMA - Gesellschaft für Chemische Technik und Biotechnologie e.V., Frankfurt, Germany. Available online:, 978-3-89746-196-2. https://bit.ly/2W3q5Ab. (Accessed 24 April 2019).

Dii, 2014. 2050 Desert Power: Getting Connected – Starting the Debate for the Grid Infrastructure for a Sustainable Power Supply in EUMENA. Dii GmbH, Munich. Available online: https://goo.gl/P17cg9. (Accessed 1 March 2019).

Dunn, B., Kamath, H., Tarascon, J.-M., 2011. Electrical energy storage for the grid: a battery of choices. Science 334, 928–935.

[EC] – European Commission, 2014. ETRI 2014 - Energy Technology Reference Indicator Projections for 2010–2050. Petten, Netherlands. Available online: https://setis.ec.europa.eu/system/files/ETRI_2014.pdf. (Accessed 24 January 2019).

[EC] – European Commission, 2015. Overview of the market segmentation for hydrogen across potential customer groups, based on key application areas. Brussels, Belgium. Available online: https://goo.gl/ETjSeS. (Accessed 24 February 2019).

Egli, F., Steffen, B., Schmidt, T.S., 2018. A dynamic analysis of financing conditions for renewable energy technologies. Nature Energy 3, 1084–1092.

ENERCON GmbH, 2014. ENERCON product overview; ENERCON GmbH: Aurich, Germany. Available online: https://goo.gl/TKdTPE. (Accessed 6 November 2016).

[ETIP-PV] – European Technology & Innovation Platform – Photovoltaic, 2017. The True Competitiveness of Solar PV – a European Case Study. ETIP-PV, Munich, March. 29. Available online: https://goo.gl/UjyGuU. (Accessed 22 December 2018).

[ETIP-PV] – European Technology & Innovation Platform – Photovoltaic, 2019. PV the Cheapest Electricity Source Almost Everywhere, ETIP-PV. Munich, May 29. Available online: https://etip-pv.eu/publications/fact-sheets/. (Accessed 30 May 2019).

ETOGAS GmbH, 2013. Power to Gas: Intelligente Konvertierung und Speicherung von Energie in der Industriellen Umsetzung. ETOGAS GmbH, Stuttgart, Germany.

EUTurbines, 2019. The gas turbine industry's commitments to drive the transition to renewable-gas power generation. EUTurbines, Brussels. Available online: https://bit.ly/2MGVx58. (Accessed 2 August 2019).

Farfan, J., Breyer, C., 2017. Structural changes of global power generation capacity towards sustainability and the risk of stranded investments supported by a sustainability indicator. J. Clean. Prod. 141, 370–384.

Fasihi, M., Bogdanov, D., Breyer, C., 2017. Long-term hydrocarbon trade options for the Maghreb region and Europe – renewable energy based synthetic fuels for a net zero emissions world. Sustainability 9 (306), 2017.

Fasihi, M., Efimova, O., Breyer, C, 2019. Techno-economic assessment of CO2 direct air capture plants. J. Clean. Prod. 224, 957–980.

Fischedick, M., Marzinkowski, J., Winzer, P., Weigel, M., 2014. Techno-economic evaluation of innovative steel production technologies. J. Clean. Prod. 84, 563–580.

Fortum, 2018a. Fortum Won the Right to Build 250 MW Solar Power Plant in India. Investor News. Fortum Corporation, Espoo, June 29. Available online: https://bit.ly/2VZ1a40. (Accessed 13 May 2019).

Fortum, 2018b. Fortum Wins the Right to Build a 250 MW Solar Power Plant in India. Investor News, Fortum Corporation, Espoo, December 21. Available online: https://bit.ly/2HVeVHH. (Accessed 13 May 2019).

Gao, J., 2019. Global Population Projection Grids Based on Shared Socioeconomic Pathways (SSPs), Downscaled 1-km Grids, 2010-2100. NASA Socioeconomic Data and Applications Center (SEDAC), Palisades, NY.

Gasworld, 2007. Oxygen global market report. Gasworld, Truro, United Kingdom. Available online: https://www.gasworld.com/oxygen-global-market-report/1277.article. (Accessed 10 March 2019).

Gerlach, A., Stetter, D., Schmid, J., Breyer, C., 2011. PV and wind power-—complementary technologies. In: Proceedings of the 26th European Photovoltaic Solar Energy Conference (EU PVSEC), Hamburg, Germany, 5–9 September. Available online: https://goo.gl/ERHmSm. (Accessed 6 November 2016).

Giuliano, S., Puppe, M., Schenk, H., Hirsch, T., Moser, M., Fichter, T., Kern, J., Trieb, F., Engelhard, M., Hurler, S., Weigand, A., Brakemeier, D., Kretschmann, J., Haller, U., Klingler, R., Breyer, C., Afanasyeva, S., 2016. THERMVOLT – Systemvergleich von solarthermischen und photovoltaischen Kraftwerken für die Versorgungssicherheit, Abschlussbericht. German Aerospace Center, Fichtner GmbH, M+W Germany GmbH, Lappeenranta University of Technology, Stuttgart, Lappeenranta. December 31.

Grond, L., Schulze, P., Holstein, J., 2013. Systems Analyses Power to Gas. KEMA NV, Groningen, the Netherland. Available online: https://bit.ly/2JDBgMn. (Accessed 14 May 2019).

Gulagi, A., Bogdanov, D., Breyer, C., 2018. The role of storage technologies in energy transition pathways towards achieving a fully sustainable energy system for India. Journal on Energy Storage 17, 525–539.

Gulagi, A., Bogdanov, D., Fasihi, M., Breyer, C., 2017. Can Australia power the energy hungry Asia with renewable energy? Sustainability 9 (233), 2017.

Gunnarsson, I., Aradóttir, E.S., Oelkers, E.H., Clark, D.E., þor Arnarson, M., Sigfússon, B., Snæbjörnsdóttir, S.Ó., Matter, J.M., Stute, M., Júlíusson, B.M., Gíslason, S.R., 2018. The rapid and cost-effective capture and subsurface mineral storage of carbon and sulfur at the CarbFix2 site. International Journal of Greenhouse Gas Control 79, 117–126.

Hansen, K., Breyer, C., Lund, H., 2019. Status and perspectives on 100% renewable energy systems. Energy 175, 471–480.

Heuser, P., Ryberg, D.S., Grube, T., Robinius, M., Stolten, D., 2019. Techno-economic analysis of a potential energy trading link between Patagonia and Japan based on CO2 free hydrogen. Int. J. Hydrogen Energy 44, 12733–12747.

Huld, T., Súri, M., Dunlop, E.D., 2008. Geographical variation of the conversion efficiency of crystalline silicon photovoltaic modules in Europe. Prog. Photovolt. Res. Appl. 16, 595–607.

IEA, 2008. World Energy Outlook 2008. International Energy Agency, Paris.

IEA, 2009. World Energy Outlook 2009. International Energy Agency, Paris.

IEA, 2015. Technology Roadmap - Hydrogen and Fuel Cells. International Energy Agency, Paris.

IEA, 2016. World Energy Outlook 2016. International Energy Agency, Paris.

IEA Bioenergy, 2017. Bioenergy's Role in Balancing the Electricity Grid and Providing Storage Options – an EU Perspective. IEA Energy Technology Network. February. Available online. https://bit.ly/2kO9TW9 (Accessed on 31 August 2019).

IEA, 2018. World Energy Outlook 2018. International Energy Agency, Paris.

IEA, 2019. The Future of Hydrogen - Seizing Today's Opportunities. International Energy Agency, Paris.

IHA, 2019. Hydropower Status Report - Sector Trends and Insights. International hydropower Association, London.

Intratec, 2018. Oxygen Price History & Forecast. Intratec Solutions LLC, Houston, USA. Website: https://www.intratec.us.

IPCC, 2012. Renewable Energy Sources and Climate Change Mitigation. Cambridge University Press, Cambridge, United Kingdom and New York, NY, USA. Available online: https://www.ipcc.ch/report/renewable-energy-sources-and-climate-change-mitigation/. (Accessed 2 August 2019).

IPCC, 2018. Special report—global warming of 1.5 °C. Intergovernmental panel on climate change. Geneva. Available online: http://www.ipcc.ch/report/sr15/. (Accessed 13 May 2019).

[ITRPV] – International Technology Roadmap for Photovoltaic, 2019. ITRPV report, Frankfurt, March. Available online: https://itrpv.vdma.org/ueber-uns. (Accessed 13 May 2019).

IRENA, 2017. Geothermal Power: Technology Brief. International Renewable Energy Agency, Abu Dhabi. September.

Jacobson, M.Z., Delucchi, M.A., Cameron, M.A., Mathiesen, B.V., 2018. Matching demand with supply at low cost in 139 countries among 20 world regions with 100% intermittent wind, water, and sunlight (WWS) for all purposes. Renew. Energy 123, 236−248.

Kawasaki, 2015. Kawasaki Develops Low-NOx Hydrogen-Fueled Gas Turbine Combustion Technology. Kawasaki Heavy Industries, Tokyo, Japan, 21 December. Available online: https://goo.gl/NMr8f8. (Accessed 4 January 2018).

Knoema, 2019. Cost of Oil Production by Country. Knoema, Washington, United States. Online source: https://knoema.com/vyronoe/cost-of-oil-production-by-country. (Accessed 24 April 2019).

Ludwig, D., Breyer, C., Seguin, R., 2019. Evaluation of an On-Site Integrated Hybrid PV-Wind Power Plant (submitted for publication).

Makridis, S.S., 2016. Hydrogen storage and compression (chapter 1). In: Carriveau, R., Ting, D.S.-K. (Eds.), Methane and Hydrogen for Energy Storage. IET Digital Library. https://doi.org/10.1049/PBPO101E_ch1.

Mason, J.E., Archer, C.L., 2012. Baseload electricity from wind via compressed air energy storage (CAES). Renew. Sustain. Energy Rev. 16, 1099−1109.

MathWorks, 2016. MATLAB and Statistics Toolbox Release 2016a. Inc.: Natick. MA, USA.

MHPS, 2018. 100% Hydrogen Power Generation—Achieving a Complete Hydrogen-Fired Gas Turbine. Mitsubishi Hitachi Power Systems, vol. 26. April, Yokohama, Kanagawa, Japan. Available online: https://goo.gl/6TQmp9. (Accessed 4 January 2018).

Michalski, J., Bünger, U., Crotogino, F., Donadei, S., Schneider, G.-S., Pregger, T., Cao, K.-K., Heide, D., 2017. Hydrogen generation by electrolysis and storage in salt caverns: potentials, economics and systems aspects with regard to the German energy transition. Int. J. Hydrogen Energy 42, 13427−13443.

Millet, P., Grigoriev, S., 2013. Chapter 2 - water electrolysis technologies. In: Gandía, L.M., Arzamendi, G., Diéguez, P.M. (Eds.), Renewable Hydrogen Technologies. Elsevier, Amsterdam, pp. 19−41.

Mosek, 2018. The MOSEK Optimization Toolbox for MATLAB Manual. Mosek ApS, Copenhagen, Denmark version 8.1.0.34.

Neij, L., 2008. Cost development of future technologies for power generation—a study based on experience curves and complementary bottom-up assessments. Energy Policy 36, 2200−2211.

NEL, 2017. Nel Quarterly Presentations − Nel ASA Q3 2017. Nel, Oslo, Norway. Available online: https://bit.ly/2PBNiGY. (Accessed 24 April 2019).

Otto, A., Robinius, M., Grube, T., Schiebahn, S., Praktiknjo, A., Stolten, D., 2017. Power-to-steel: Reducing CO_2 through the integration of renewable energy and hydrogen into the German steel industry. Energies 10, 451.

Ozarslan, A., 2012. Large-scale hydrogen energy storage in salt caverns. Int. J. Hydrogen Energy 14265−14277.

Pfenninger, S., Keirstead, J., 2015. Comparing concentrating solar and nuclear power as baseload providers using the example of South Africa. Energy 87, 303−314.

Pitz-Paal, R., 2017. Concentrating solar power systems. EPJ Web Conf. 148, 00008.

Pogge von Strandmann, P.A.E., Burton, K.W., Snæbjörnsdóttir, S.O., Sigfússon, B., Aradóttir, E.S., Gunnarsson, I., Alfredsson, H.A., Mesfin, K.G., Oelkers, E.H., Gislason, S.R., 2019. Rapid CO2 mineralisation into calcite at the CarbFix storage site quantified using calcium isotopes. Nat. Commun. 10, 1983.

Ram, M., Bogdanov, D., Aghahosseini, A., Gulagi, A., Oyewo, A.S., Child, M., Caldera, U., Sadovskaia, K., Farfan, J., Barbosa, L.S.N.S., Fasihi, M., Khalili, S.,

Dahlheimer, B., Gruber, G., Traber, T., De Caluwe, F., Fell, H.-J., Breyer, C., 2019. Global Energy System Based on 100% Renewable Energy − Power, Heat, Transport and Desalination Sectors, Study by LUT University and Energy Watch Group, Lappeenranta, Berlin, April 12, ISBN 978-952-335-339-8. Available online: https://bit.ly/2UJmUAP. (Accessed 24 April 2019).

Ram, M., Child, M., Aghahoseeini, A., Bogdanov, D., Lohrmann, A., Breyer, C., 2018. A comparative analysis of electricity generation costs from renewable, fossil fuel and nuclear sources in G20 countries for the period 2015-2030. J. Clean. Prod. 199, 687−704.

Reichenberg, L., Hedenus, F., Odenberger, M., Johnsson, F., 2018. Tailoring large-scale electricity production from variable renewable energy sources to accommodate baseload generation in Europe. Renew. Energy 129, 334−346.

Samsung, S.D.I., 2018. Energy Storage System - Battery Business. Samsung SDI Co. Ltd., Yongin-si, South Korea. March. Available online: https://bit.ly/2D62yGs. (Accessed 31 August 2019).

Sepulveda, N.A., Jenkins, J.D., de Sisternes, F.J., Lester, R.K., 2018. The role of firm low-carbon electricity resources in deep decarbonization of power generation. Joule 2, 1−18.

Shokrzadeh, S., Jafari Jozani, M., Bibeau, E., Molinski, T., 2015. A statistical algorithm for predicting the energy storage capacity for baseload wind power generation in the future electric grids. Energy 89, 793−802.

Short, W., Packey, D.J., Holt, T., 1995. A Manual for the Economic Evaluation of Energy Efficiency and Renewable Energy Technologies, vol. 1995. National Renewable Energy Laboratory (NREL), Golden, CO, USA. Available online: https://goo.gl/aD6zjn. (Accessed 4 January 2019).

Siemens, 2019. Hydrogen Combustion in Siemens Gas Turbines - Sales Information v2.0. Siemens AG, Munich, April.

Solomon, A.A., Bogdanov, D., Breyer, C., 2019. Curtailment-storage-penetration nexus in the energy transition. Appl. Energy 235, 1351−1368.

Squalli, J., 2017. Renewable energy, coal as a baseload power source, and greenhouse gas emissions: evidence from U.S. state-level data. Energy 127, 479−488.

Stackhouse, P., Whitlock, C. (Eds.), 2008. Surface Meteorology and Solar Energy (SSE) Release 6.0 Methodology. National Aeronautic and Space Administration (NASA), Langley, VA, USA.

Stackhouse, P., Whitlock, C. (Eds.), 2009. Surface Meteorology and Solar Energy (SSE) Release 6.0 Methodology. National Aeronautic and Space Administration (NASA), Langley, VA, USA.

Stetter, D., 2012. Enhancement of the REMix Energy System Model: Global Renewable Energy Potentials, Optimized Power Plant Siting and Scenario Validation. Ph.D. Thesis, Faculty of Energy-, Process- and Bio-Engineering, University of Stuttgart, Stuttgart, Germany.

Teske, S. (Ed.), 2019. Achieving the Paris Climate Agreement Goals - Global and Regional 100% Renewable Energy Scenarios with Non-energy GHG Pathways for +1.5°C and +2°C. Springer International Publishing, New York. https://doi.org/10.1007/978-3-030-05843-2.

Trieb, F., Schillings, C., Kronshage, S., Viebahn, P., May, N., Paul, C., 2006. In: Trans-Mediterranean Interconnection for Concentrating Solar Power. German Aerospace Center (DLR), Stuttgart. www.dlr.de/tt/trans-csp.

UNFCCC, 2015. Adoption of the Paris Agreement—Proposal by the President. United Nations Framework Convention on Climate Change Paris, France.

Valera-Medina, A., 2018. Ammonia for power. Prog. Energy Combust. Sci. 69, 63−102.